Department of Automation and Systems Technology

Advanced Process Monitoring and Control Methods in Mineral Processing Applications

Antti Remes

Aalto University

DOCTORAL DISSERTATIONS

Aalto University publication series
DOCTORAL DISSERTATIONS 17/2012

Advanced Process Monitoring and Control Methods in Mineral Processing Applications

Antti Remes

Doctoral dissertation for the degree of Doctor of Science in Technology to be presented with due permission of the School of Electrical Engineering for public examination and debate in Auditorium AS1 at the Aalto University School of Electrical Engineering (Espoo, Finland) on the 16th of March 2012 at 12 noon (at 12 o'clock).

Aalto University
School of Electrical Engineering
Department of Automation and Systems Technology
Control Engineering

Supervisor
Emeritus Prof. Heikki Koivo

Instructor
Emeritus Prof. Heikki Koivo

Preliminary examiners
Prof. Pertti Lamberg, Luleå University of Technology, Sweden
Prof. Sirish Shah, University of Alberta, Canada

Opponents
Prof. Kauko Leiviskä, University of Oulu, Finland
Prof. Sirish Shah, University of Alberta, Canada

Aalto University publication series
DOCTORAL DISSERTATIONS 17/2012

ISBN 978-952-60-4511-5 (printed)
ISBN 978-952-60-4512-2 (pdf)
ISSN-L 1799-4934
ISSN 1799-4934 (printed)
ISSN 1799-4942 (pdf)

Unigrafia Oy
Helsinki 2012

Finland

The dissertation can be read at http://lib.tkk.fi/Diss/

441 697
Printed matter

Author
Antti Remes

Name of the doctoral dissertation
Advanced Process Monitoring and Control Methods in Mineral Processing Applications

Publisher School of Electrical Engineering

Unit Department of Automation and Systems Technology

Series Aalto University publication series DOCTORAL DISSERTATIONS 17/2012

Field of research Control Engineering

Manuscript submitted 13 June 2011 **Manuscript revised** 20 December 2011

Date of the defence 16 March 2012 **Language** English

☐ **Monograph** ☒ **Article dissertation (summary + original articles)**

Abstract

In minerals processing the high material volumes yield the fact that benefits of even small improvements in the process efficiency are remarkable. On a daily basis, the efficiency of a concentrating plant relies on the performance of the process control system, and secondly, on the adequate information of the process state provided for the plant operators. This thesis addresses the problems in the monitoring and control of the selected, widely applied mineral concentration unit processes and the processing circuits. The case studies cover operations in the ore grinding stages, including size separation units, followed subsequently by the concentration and the thickening stages in the downstream process. The developed methods and applications are all verified with industrial data, industrially identified models or by the practical implementations and tests on the industrial case plants.

Advanced control systems - including a rule-based, a fuzzy and a model predictive control, with different combinations and setups - are studied with simulated grinding and flotation processes. A new model-based expert system for controlling of the ground ore particle size and the circulating load of the grinding process is proposed. The system was tested with a simulation model representing an industrial milling of apatite ore.

In a plant-wide process monitoring, a data-based modeling approach is applied to predict the concentrate quality and the impact of the grinding stage parameters on that. The plant model, used for the monitoring, is updated adaptively; this enables timely information on the process. The monitoring system was set up based on the data of a chromite ore processing plant.

Two unit operations, a hindered settling separator and a thickener, were modeled from a viewpoint of equipment monitoring and control purposes. The hindered settling separator incorporates both a mechanistic particle-settling model and a separation efficiency characterization curve in a novel manner. Separation characteristics in a pyrite concentrate case and in a ground apatite ore case were studied with the model. Operation of a thickener was modeled based on on-line mass-balance estimation. The monitoring application was implemented in an industrial apatite concentrate thickener.

This thesis demonstrates the benefits of the above described monitoring and control methods. The metallurgical performance improvements are pointed out for each case. Also this thesis outlines the practical implementation and robustness issues for the methods. Thus the thesis promotes the advantages of more extensive use of plant models in process operation purposes.

Keywords minerals processing, mining, modeling, simulation, control, optimisation

ISBN (printed) 978-952-60-4511-5 **ISBN (pdf)** 978-952-60-4512-2

ISSN-L 1799-4934 **ISSN (printed)** 1799-4934 **ISSN (pdf)** 1799-4942

Location of publisher Espoo **Location of printing** Helsinki **Year** 2012

Pages 170 **The dissertation can be read at** http://lib.tkk.fi/Diss/

Aalto-yliopisto

Tiivistelmä

Aalto-yliopisto, PL 11000, 00076 Aalto www.aalto.fi

Tekijä
Antti Remes

Väitöskirjan nimi
Rikastusprosessien moderni säätö ja monitorointi

Julkaisija Sähkötekniikan korkeakoulu

Yksikkö Automaatio- ja systeemitekniikan laitos

Sarja Aalto University publication series DOCTORAL DISSERTATIONS 17/2012

Tutkimusala Systeemitekniikka

Käsikirjoituksen pvm 13.06.2011 **Korjatun käsikirjoituksen pvm** 20.12.2011

Väitöspäivä 16.03.2012 **Kieli** Englanti

☐ **Monografia** ☒ **Yhdistelmäväitöskirja (yhteenveto-osa + erillisartikkelit)**

Tiivistelmä

Mineraalien rikastusprosessissa käsitellään tyypillisesti hyvin suuria materiaalivirtoja. Tästä johtuen jo pienetkin parannukset prosessin tehokkuudessa ovat merkittäviä. Päivittäisessä rikastamon toiminnassa laitoksen suorituskyky pohjautuu prosessin ohjausjärjestelmän suorituskykyyn, sekä siihen miten tarkoituksenmukaista ja oikea-aikaista tietoa prosessin tilasta pystytään prosessioperaattoreille välittämään. Tässä väitöskirjassa käsitellään monitorointi- ja ohjausongelmia tietyille yleisille rikastamon yksikköprosesseille ja prosessipiireille. Tarkasteltavat prosessit ja prosessointivaiheet käsittävät malmin jauhatuksen sekä siihen liittyviä luokituslaitteita, seuraavana prosessiketjussa olevia erityyppisiä mineraalien rikastuspiirejä ja prosessin loppupäässä vedenpoistoa varten olevan lietteen sakeutuksen. Kaikki kehitetyt menetelmät ovat testattu teollisella datalla, teollisten prosessien malleilla tai käytännön prosessikokeilla sekä menetelmien käyttöönotolla rikastamolaitoksella.

Kehittyneitä ohjausjärjestelmiä – käsittäen sääntökanta-, sumean- ja mallinprediktiivisen ohjauksen – on tarkasteltu simuloitujen jauhatus- ja vaahdotuspiirien avulla. Tämän tuloksena on esitetty uusi mallipohjainen asiantuntijajärjestelmä jauhetun malmin raekoon sekä jauhatuspiirin kiertokuorman ohjaamiseksi. Tätä järjestelmää on testattu teollista apatiittimalmin jauhatuspiiriä kuvaavalla simulaattorilla.

Datapohjaista mallintamista on myös sovellettu rikastamon kattavassa monitorointisovelluksessa, jolla ennustetaan rikasteen laatu jauhatusvaiheen parametrien perusteella. Monitoroinnissa käytettyä rikastamon mallia päivitetään jatkuvatoimisesti; siten on mahdollista saada oikea-aikaista tietoa prosessin tilasta ajotilanteiden muuttuessa. Testattu järjestelmä perustuu kromiittimalmin rikastamodataan.

Tutkituista yksikköoperaatioista on mallinnettu sekä hidastettuun laskeutumiseen perustuva erotus että sakeutus siten että mallit soveltuvat laitteen monitorointiin ja ohjaukseen. Hidastetun partikkelien laskeutumisen malli käsittää sekä mekanistisen- että erotusterävyysmallin, jotka on tässä yhdistetty uudella tavalla. Tällä mallilla on tutkittu sekä rikkikiisurikasteen että jauhetun apatiittimalmin erotusominaisuuksia. Sakeuttimeen on puolestaan sovellettu jatkuvatoimista massataseen määritystä. Monitorointisovellus on toteutettu teollisen apatiittirikasteen sakeuttimeen.

Väitöskirja osoittaa edellä kuvattujen monitorointi- ja ohjausmenetelmien edut. Nämä on esitetty tarkasteltavien prosessien metallurgisen suorituskyvyn muutoksina. Lisäksi tässä työssä käsitellään menetelmien käytännön toteutukseen ja toimintavarmuuteen liittyviä näkökohtia. Tämän väitöskirjan tulokset tukevat laajamittaista prosessimallien käyttöä ja

Avainsanat mineraalien käsittely, kaivokset, mallinnus, simulointi, optimointi

ISBN (painettu) 978-952-60-4511-5 **ISBN (pdf)** 978-952-60-4512-2

ISSN-L 1799-4934 **ISSN (painettu)** 1799-4934 **ISSN (pdf)** 1799-4942

Julkaisupaikka Espoo **Painopaikka** Helsinki **Vuosi** 2012

Sivumäärä 170 **Luettavissa verkossa osoitteessa** http://lib.tkk.fi/Diss/

Preface

The research work for this thesis was performed mainly in Control Engineering Research Group at Aalto University. I joined the group in early 2007, under guidance and supervision of Prof. Heikki Koivo. Especially, I would like to thank him for the years in the inspiring and encouraging work atmosphere that he created.

The research project related to this thesis was supported by The Finnish Funding Agency for Technology and Innovation (TEKES) during 2007-2009. In addition, the industrial collaboration with the Pyhäsalmi Mine Oy, Outokumpu Chrome Oy and Yara Siilinjärvi mine forms the core basis for this thesis. I warmly thank the staff of all of the mines, as well as Dr. Kari Saloheimo from Outotec for supporting and providing ideas during the research work.

I have been supported financially for the research by the Finnish Foundation for Economic and Technology Sciences - KAUTE, the Finnish Foundation for Technology Promotion, the Outokumpu Foundation, the Walter Ahlström Foundation, the Emil Aaltonen Foundation, the 30th Anniversary Foundation of Neles Inc. and the Finnish Society of Automation. Their support is gratefully acknowledged.

The pre-examination of the thesis was carried out by Prof. Pertti Lamberg from the Luleå University of Technology and Prof. Sirish Shah from the University of Alberta. The valuable comments and professional support for the mineral processing topics are highly appreciated. Also, I would like to thank Mr. William Martin for proofreading of the manuscript. Thanks also go to the whole research group's personnel for creative discussions and in particular for Mr. Pauli Sipari and Dr. Jani Kaartinen for co-working in project related practical issues. Finally, major thanks belong to my friends and family who encouraged me to keep going on during the years.

Antti Remes

List of Publications

P1 Remes, A., Vaara, N., Jämsä-Jounela, S.-L. (2006). Analysis of industrial grinding circuits using PCA, PLS and neural networks, *IFAC Workshop on Automation in Mining, Minerals and Metal Industry*, 20.-22. Sept 2006, Cracow, Poland.

P2 Remes, A., Saloheimo, K., Jämsä-Jounela, S.-L. (2007). Effects of on-line elemental analysis speed and accuracy on flotation control performance, *Miner. Eng.*, **20**, pp. 1055-1055.

P3 Remes, A., Vaara, N., Saloheimo, K., Koivo, H. (2008). Prediction of Concentrate Grade in Industrial Gravity Separation Plant – Comparison of rPLS and Neural Network, *Proceedings of the 17th IFAC World Congress*, 6.-11. Jul. 2008, Seoul, Korea, pp. 3280-3285.

P4 Remes, A., Kaartinen, J., Saloheimo, K., Vaara, N., Pekkarinen, H., Koivo, H. (2008). Monitoring of the grinding and gravity separation operation at Outokumpu's Kemi concentrator plant, *Proceedings of the XXIV International Mineral Processing Congress*, 24.-28. Sep. 2008, Beijing, China, pp. 2438-2447.

P5 Moilanen, J., Remes, A. (2008). Control of Flotation Process, *Proceedings of V International Mineral Processing Seminar*, 22-24. Oct 2008, Santiago, Chile, pp. 317-325.

P6 Remes, A., Aaltonen, J., Koivo, H. (2009). Soft-sensor estimation of an apatite thickener operation at the Siilinjärvi concentrator, *Pre-prints of IFAC Workshop on Automation in Mining, Minerals and Metal Industry*, 14.-16. Oct. 2009, Viña del Mar, Chile, 6 p.

P7 Remes, A., Aaltonen, J., Koivo, H. (2010). Grinding Circuit Modeling and Study of the Particle Size Control at the Siilinjärvi Concentrator, *Int. J. Miner. Process.*, **96**, pp. 70-78.

P8 Remes, A., Tuikka. A., Koivo, H. (2011). Simulation and pilot experiments of pyrite concentrate separation in Floatex density separator, *Miner. Metall. Proc.*, **28**, pp.62-70.

Contributions of the Author – Publications

P1 The author wrote the article. The experimental work at the Outokumpu Tornio Works Kemi concentrator described in the article was carried out both by the author and the Kemi plant personnel. Especially M.Sc Niina Vaara was largely responsible for the process experiments.

P2 The author wrote the article together with Dr. Kari Saloheimo, with support of prof. Jämsä-Jounela. The results covering the topics of this Thesis are presented in Chapter 3 of the article. The presented process simulations and analysis of the results are carried out by the author.

P3 The author wrote the article, the process modeling work was advised by prof. Koivo and Dr. Saloheimo. The plant data was obtained based on the work presented in the article [P1].

P4 The author wrote the article and carried out the data-analysis. Dr. Jani Kaartinen supported with the automation system configuration tasks at the Kemi concentrator. M.Sc. Niina Vaara supervised the mill control experiments and provided supplemental data and process knowledge. Dr. Saloheimo, M.Sc. Pekkarinen and prof. Koivo contributed by reviewing and advising in the writing phase of the article.

P5 The author carried out the control simulations and wrote the Sections covering that in the article. Rest of the article was written by Mr. Jari Moilanen.

P6 The author wrote the article and carried out the presented development work. The experimental work at the Siilinjärvi concentrator was carried out under the supervision of Mr. Jarmo Aaltonen.

P7 The author wrote the article and carried out the presented modeling and control simulation work. The process

experiments were carried out by the author together with the Siilinjärvi plant personnel, especially with Mr. Jarmo Aaltonen.

P8 The author wrote the article and performed the modeling and the data analysis related to that. Mr. Aki Tuikka supervised the pilot experiments, carried out by the Pyhäsalmi plant personnel, and provided the preprocessed data and other supplemental process information.

Nomenclature

A	Parameter in separation efficiency function
A_{cell}	Cross sectional area inside floatation cell
$A_{floatex}$	Cross sectional area inside FSD
Ar	Archimedes number
A_s	Aspect ratio of flotation cell impeller
a	Fitted parameter in water recovery formula
$\boldsymbol{B}_{\mathrm{R}}$	Matrix of regression coefficient
$\boldsymbol{B}_{\mathrm{RLS}}$	Matrix of least squares regression coefficients
B_{br}	Breakage function
B	Parameter in separation efficiency
b	Fitted parameter in water recovery formula
$\boldsymbol{C}$	Matrix of loadings (Y-block)
$C_{D,ij}$	Drag coefficient of a particle
c	Parameter in separation efficiency function
c_s	Solids concentration in thickener
$D50$	50% passing size of slurry
d	Rank of matrix
d_b	Bubble size in flotation cell
d_i	Particle mean diameter in size class i
d_p	Diameter of a particle
$d_{p,ij}$	Mean size of particles in the density and size fraction class
d_{50}	Separation cut size
Ent	Entrainment factor in flotation
$\boldsymbol{e}_t$	Error between the PLS estimate and the measurement
F	Feed mass flow rate
F_{teeter}	Teeter water flow rate
F_{80}	80% passing size of solids
f	Feed particle size distribution function
f_{ij}	Feed density and size composition (of FSD)
G	Total downwards solids flux in thickener
$G_{ij}(s)$	Process transfer function
G_s	Settling flux of solids in thickener
G_t	Transport flux of solids in thickener
g	Acceleration due gravity
H_f	Froth height in flotation cell

$H_{f,max}$	Froth height (maximum) where all bubbles are bursting
h	Depth of the froth over the launder lip in flotation cell
h_t	Height of thickener
i	Index variable
J	Cost function in MPC
J_g	Superficial gas velocity in flotation cell
j	Index variable
K	Kalman gain
k	Kinetic rate constant of flotation
k_c	Kinetic rate constant of flotation cell collection zone
l	Number of latent variables
l_l	Length of flotation cell launder lip
m	Number of predictor variables
$\dot{m}_n$	Mass flow rate of line *n* in thickener
m_{solids}	Solids mass in thickener
m_{water}	Water mass in thickener
N_o	Memory length in adaptive forgetting factor
N_s	Flotation cell impeller peripheral speed
n	Number of predicted variables
ne	Prediction horizon length in MPC
n_{ij}	Richardson-Zaki index of a particle
nu	Control horizon length in MPC
O	Overflow mass flow rate
o_{ij}	Overlfow density and size composition (of FSD)
$\boldsymbol{P}$	Matrix of loadings (X-block)
P	Ore specific floatability
P_m	Measured pressure in fludization bed
$P_{waterbed}$	Pressure of water filled FSD
P_{80}	80% passing size of solids
$\boldsymbol{p}$	Vector of loadings (X-block)
p	Product particle size distribution
$p_{underflow_{cone}}$	Pressure of thickener underflow cone
Q	Process covariance matrix in Kalman filter
Q_{AIR}	Volumetric air flowrate to flotation cell
R	Measurement covariance matrix in Kalman filter
R_E	Entrainment recovery
Re_t	Reynold number of a particle
R_f	Froth recovery
R_T	True flotation recovery

R_w	Water recovery in flotation
r	Bypass fraction of fines in FSD
S	Selection function
S_b	Bubble surface area flux in flotation cell
$\boldsymbol{T}$	Matrix of scores (X-block)
$\boldsymbol{t}$	Vector of scores (X-block)
t	Time variable
$\boldsymbol{U}$	Matrix of scores (Y-block)
U	Underflow mass flow rate
$U_{t,ij}$	Terminal settling velocity of a particle
u	Process input
u_f	Downward fluid velocity in thickener, process input
u_{ij}	Underflow density and size composition (of FSD)
V_{ij}	Slip velocity of a particle
$V_{thickener}$	Volume of thickener
v_l	Froth velocity in flotation cell
$\dot{v}_n$	Volumetric flow rate of line *n* in thickener
$\dot{v}_{overflow}$	Volumetric flow rate of overflow water of thickener
$v_{teeter.int}$	Interstitial teeter water velocity
$v_{teeter.sup}$	Superficial teeter water velocity
$\dot{v}_{water,n}$	Volumetric flow rate of water of line *n* in thickener
$\dot{v}_{water_{addition}}$	Volumetric flow rate of water addition to thickener cone
$\boldsymbol{W}^*$	Matrix of PLS predictor weights
W	Work input of the grinding mills
WIo	Bond operating work index
$\boldsymbol{w}^*$	Vector of PLS predictor weights
$\boldsymbol{X}$	Matrix of predictor variables
$\hat{x}$	A-posteriori states in Kalman filter
$\hat{x}\_$	A-priori states in Kalman filter
$\boldsymbol{Y}$	Matrix of predicted variables
$\widehat{\boldsymbol{Y}}$	Matrix of estimated predicted variables
y	Process output
$\hat{y}$	Predicted output in MPC
y_p	Uncorrected efficiency curve
y_p'	Separation efficiency
y_r	Output reference in MPC
Z	Height of solid-liquid interface in thickener sedimentation

α	Air recovery in flotation cell
γ_y	Output weightings for the control error in MPC
γ_u	Input weightings for the control increments in MPC
Δu	Control increment in MPC
δ	Drainage parameter of coarse particles
ε_{avg}	Average voidage of fluidization bed
λ_{air}	Air residence time in flotation froth phase
$\lambda_{\min}$	Minimum limit of forgetting factor of recursive PLS
λ_t	Forgetting factor of recursive PLS
μ_{water}	Viscosity of water
ξ	Particle cut size having 20% entrainment
$\rho_{avg.particle}$	Average density of particles in fluidization bed
ρ_f	Density of feed flow
ρ_{ij}	Density of a particle
ρ_{solids}	Solids density
ρ_{sus}	Average density of suspension
$\rho_{thickener}$	Average slurry density in thickener
ρ_{water}	Density of (fluidization) water
$\sigma_{v,slip}$	Standard deviation of particle slip velocity
σ_o^2	Measurement noise variance in adaptive forgetting factor
τ	Flotation cell pulp zone residence time
ψ	Sphericity of a particle
Ø	Diameter (of a Reichert cone or a thickener)

Abbreviations

AG	Autogenous Grinding
AP	Apatite
DEM	Discrete Element Method
FLG	Phlogopite
FSD	Floatex Density Separator
HGMS	High-Gradient Magnetic Separator
HR	Fine concentrate
KRB	Carbonate
MIMO	Multiple Input Multiple Output
MPC	Model Predictive Control
PID	Proportional Integral Derivative controllers
PLS	Partial Least Squares
SAG	Semi-Autogenous Grinding
TMT	Rod mill product
VMS	Volcanogenic Massive Sulphide zone
XRF	X-Ray Fluorescence

Chemical Symbols and Compounds:

Cr_2O_3	Chromite
Cu	Copper
$CuFeS_2$	Chalcopyrite
FeS_2	Pyrite
P_2O_5	Phosporus pentoxide
S	Sulphur
Zn	Zinc
$Zn_{0.95}Fe_{0.05}S$	Sphalerite

Contents

1 Introduction

1.1 Background

The mining industry has a strong indirect impact on our daily life. The end products, metals – processed from the excavated ore minerals – are utilized in a wide range of manufacture, for example in transportation vehicles, constructions, electronics and consumer goods. For instance, currently around 50 % of the copper and 70 % of the steel of the world's demands are supplied by processing the excavated ore; the rest of the material is obtained from recycling (Reuter et al., 2005). Processing of the ore is a remarkable energy consumer having both economical and environmental effects. Due to the large material flows in the ore processing, even a small percentual improvement in the operations has a significant effect annually.

In the mine sites, the mineral comminution circuits – carrying out the size reduction of the excavated ore – consume typically up to 40 % of the electrical energy; of which only 1 % is attributed to the production of new surface area of the feed ore (Pokrajcic and Morrison, 2008). In addition to the energy efficiency of the comminution circuit, the overall process efficiency is determined by the particle size distribution and mineral liberation produced by the circuit, having an impact on the downstream concentration stages. Therefore, it is obvious that good operating practices, available process monitoring techniques and well-performing control methods, especially in the comminution stage, have a significant influence on the concentrator performance.

According to the survey study of Wei and Craig (2009a and 2009b) over 60% of grinding circuits were controlled merely by PID (Proportional Integral Derivative) control. Multivariable and expert systems were applied in 20% of cases while the frequency of model predictive control cases was less than 10%. A brief description of commonly applied grinding process measuring, modeling, monitoring and also control techniques is given in Hodouin (2010). The author also suggests that when the control performance of a grinding circuit is evaluated, the impact on the subsequent concentration circuit should definitely be taken into account.

Monitoring and Control of Grinding Circuits

Rule-based control of the grinding circuits has been a widely applied method to handle process disturbances, typically originating from the ore feed. For example, at the Ok Tedi Mining the frequent and drastic ore type

and feed size variations have been tackled by gradual long-term development of a rule-based and fuzzy expert system for the SAG mill control, allowing increased throughput (McCaffery et al., 2002). Also rule-based particle size control with encouraging results has been reported by Yianatos et al. (2002). From elsewhere, Duarte et el. (2001) pointed out the advantages of neural control in varying operating conditions, using a simulated Codelco-Andina grinding plant. In addition, Duarte et al. (1998) have performed a multivariable control test at the Codelco-Andina copper concentrator grinding section. Lestage et al. (2002) applied linear programming for finding the optimal ore feed rate and sump water addition rate set points as a function of operating constraints.

In the grinding process, the ore grindability dictates largely the mill operating point and throughput. Gonzalez et al. (2008) has studied model-based grindability detection with simulations. In addition, Mitra (2009) has studied the effect of uncertainties, both in the grindability model parameters and in the data, on the optimization of both circuit throughput and the percent of mid size passing fraction. It was concluded that particularly the accuracy of the grindability index has a strong impact on the optimization problem.

Most recently, model predictive control has raised interest also in the mineral grinding applications. Several studies of model predictive control (MPC) in grinding processes have been reported: Pomerleau et al. (2000) performed a simulation study comparing different unit controller, multivariable control and model-based control scemes; Muller and de Vaal (2000) pointed out the robustness of the MPC to the model mismatches; Ramasamy et al. (2005) showed that the MPC performs better than a PI control when different operating conditions occur. Later on, Coetzee et al. (2010) have presented a nonlinear model predictive simulation control study, concluding that the practical implementation of the method is still currently unfeasible. Instead, a simulation study of a SAG mill predictive control with linear models was shown to be feasible (Garrido and Sbarbaro, 2009). Also, Apelt and Thornhill (2009) showed by simulations the advantages of the MPC compared to the PID control in mill power draw stabilization. The applied model was developed based on the Northparkers Mines SAG mill data; utilization of the estimated nonlinear mill operating curve in the control system was also proposed. Elsewhere, an industrial application described in Gatica et al. (2009) and Nieto (2009) outlined implementation of a SAG mill model predictive control, based on the transfer function models identified from the process, at the Codelco Chile El Teniente division. According to the long term operation data, the mill throughput increased on average between 2% and 6%.

Monitoring and Control of Grinding – Concentration Process Chain

Yianatos et al. (2000) simulated the grinding – flotation process chain to study the optimality in terms of the throughput, the grinding fineness and subsequently the flotation recovery. The model was calibrated with Codelco-Chile Salvador copper concentrator data; based on the results, the necessity for on-line particle size measurement was addressed. At the same time, Sosa-Blanco et al. (2000) performed a study of the flotation economics improvements by means of the grinding circuit tuning. A procedure for statistical monitoring of data from a grinding-flotation circuit was demonstrated in Groenewald et al. (2006), suggesting the inclusion of process performance indices and the model predictions into the monitoring scheme to further improve the analysis of the root causes. More recently, Wei and Craig (2009a) have still emphasized the importance of evaluating the grinding and concentration (flotation) as one assembly when different control setups are assessed. They have also performed a simulation study, demonstrating the effect of the model predictive control of a one-stage run-of-mine mill on the subsequent flotation recovery and overall performance.

1.2 Objectives and Asserted Hypothesis

Mineral processing plants have a large potential for operational performance improvements in a wide range of applications. Even if the process flowsheet has been optimized during long-term development efforts, short-time disturbances can temporarily decrease the process performance significantly. Typically these performance measures can be directly indicated in metallurgical figures such as concentrate grade and recovery, which can be – on the other hand – transformed into the economical profitability figures of the plant. This thesis addresses the issue of maintaining the process profitability by applying various process monitoring and control methods in the selected mineral processing units. The applied methods are verified by means of process experiments, data-analyses, simulations, and automation system implementations in the concentrators of three Finnish mines. The case plants are: the Outokumpu Chrome Oy Kemi Mine, the Yara Suomi Siilinjärvi Mine and the Inmet Mining Co. Pyhäsalmi Mine.

Therefore, this thesis asserts that *by applying advanced process monitoring and control techniques in a novel way throughput, quality, grade or recovery of the product of a mineral processing plant or a unit process can be greatly improved*, subsequently leading to economical improvements of the process operation. The obtained benefits for the

selected case unit processes and sequential processing stages are demonstrated and also the applicability of the methods is verified.

1.3 Scope and Contribution of the Thesis

In this thesis existing modeling, monitoring and control methods are further developed and applied in novel practices to the selected industrial case processes. The major impact of the approach is that the methods are proven to work robustly in accordance with the industrial plant tests or with industrially parameterized process models. The results are generic in the sense that the restrictions, the anticipated benefits and the work flow for the implementation procedure for other similar process cases can be outlined based on the results of this thesis.

Contributions of this thesis in order to address the asserted objectives are as follows:

- **Model-based grinding circuit control system:** Frequent changeovers of the ore feed type require timely control actions to tune the grinding circuit to act in a proper operation state. In this thesis a plant test based simulator, comprising a model-based control of ground ore particle size distribution, was set up in conjunction with an expert control scheme for the circulating load of the grinding circuit. This novel approach was tested by simulations with long term plant data.
  Case application: Siilinjärvi apatite grinding circuit.

- **Hindered settling separators:** Operation of a hindered settling separation can be difficult to stabilize when varying feed conditions are present. This can lead to an off-specification separation result, causing, for example, losses in recovery in the subsequent concentrating phase. The modeling approach, developed in this thesis, for examining the unit operation combines a slip velocity based particle movement calculation together with a separation efficiency characteristic in a novel way.
  Case applications: Pyhäsalmi pyrite pilot unit and Siilinjärvi apatite units.

- **Thickeners:** Disturbances in slurry thickening can become a bottleneck for the whole concentrating plant, if not detected and tackled at an early stage. Here, the existing process measurements are utilized in a novel manner to estimate the thickener state to detect the

upcoming faults by using the proven Kalman filtering algorithm. The operation is verified with an industrially implemented solution.
Case application: Siilinjärvi apatite concentrate thickener.

- **Plant-wide monitoring, based on adaptive data-based predictive model:** Early responses in the ore feed characteristics can reduce fluctuations in the final concentrate grade and recovery. This thesis addresses the issue with a new adaptive prediction of the concentrate quality based on grinding section measurements. The model parameters provide information on the impact of the grinding stage operating parameter on the plant results.
Case application: Kemi chromite grinding and gravity concentration.

- **Control studies of mineral beneficiation:** This thesis includes evaluation of the benefits of selected mineral processing control schemes. An expert system and model predictive control are studied with flotation simulators, a closed-loop particle size control for a grinding circuit is tested in plant operation and a grinding-flotation chain is studied with plant calibrated simulations. These evaluations pointed out economical and metallurgical impacts of the control improvements that have not been assessed before.
Case applications: generic flotation simulators, Kemi chromite grinding circuit and Pyhäsalmi grinding – copper flotation chain.

1.4 Summary of Publications

The publications handle research work covering a time span of around five years, starting in 2005. The early research stage discussed in [P2] deal with a preliminary study of an expert system and model predictive control with a model obtained from the literature. Around the same time, the first plant experiment started at the Kemi concentrator grinding section. That work and the related data analysis are described in publication [P1].

A major part of the research was carried out in the *MinMo*-project '*Advanced Methods in Monitoring and Control of Ore Concentration*' during 2007-2009. Using the data of publication [P1], a plant-wide model to predict the concentrate chromite grade based on the grinding parameters is presented in publication [P3]. Publication [P4] summarizes various monitoring and control schemes developed and tested in the Kemi case process. Elsewhere, in the Siilinjärvi plant case, a soft-sensor monitoring system for the apatite concentrate thickener was developed, tested and implemented; this is summarized in publication [P6]. Several experiments,

related modeling work and, finally, formulation of a model-based grinding control scheme were carried out at the Siilinjärvi plant. These are covered in publication [P7].

The field of flotation control [P5] and the pilot scale Floatex separator modeling [P8] are also studied. The flotation control case points out the benefits of an assay and machine vision based flotation control by means of a first principles simulator. In addition, the advantages of the feedforward flotation cell level control were demonstrated by simulations. In the other publication, [P8], a pilot scale hindered settling separator was calibrated and the operation was studied with the Pyhäsalmi pyrite experiment data. The publication is based on a similar model structure as applied earlier in the *MinMo*-project Siilinjärvi case; a slight difference is that in publication [P8] the model calibration was developed further.

1.5 Structure of the Thesis

This thesis is organized as follows. In Chapter 2 the operation principles of the mineral processing equipment related to the case processes are described from the modeling point of view. The description is relatively extensive since it forms the basis for the understanding of the characteristics of the case processes. Chapter 3 reviews the key methodology applied in the monitoring and control schemes of the thesis. The case concentrator plants - located in Kemi, Siilinjärvi and Pyhäsalmi – are introduced in Chapter 4. The description summarizes briefly the mine history, geology and the production. The process experiments, the application setups and the obtained results are presented in Chapter 5. The chapter starts with a description of the experiments and data sampling in each case, followed by the modeling and monitoring of the unit processes. Next the plant-wide monitoring case is described and finally the control studies are presented. Chapter 6 provides a conclusion of the work summing up the benefits, challenges and future prospects of the schemes applied and developed in this thesis.

2 Operation and Models of Selected Mineral Beneficiation Equipment

After mining the ore is further processed in a concentrator plant. The main milling stages are: (i) *liberation* of the valuable minerals from the gangue and then, (ii) *separation* of them into concentrate and tailings streams (Wills and Napier-Munn, 2006). Liberation of the minerals is achieved by applying size reduction techniques. Machines for the size reduction of solid pieces are commonly based on four major effects; compression, impact, rubbing and cutting (McCabe, et al., 1993). In concentrators, the *comminution* process covers at least the *crushing* and typically also the *grinding* stages. In addition, the comminution stage often includes size classification equipments, such as screens and cyclones. The subsequent separation, or *concentration* of the ore, is commonly carried out with some physical methods, such as *froth flotation* and *gravity separation*. In case of solids-water slurry mixtures, the next process stage is *dewatering*, which typically includes *gravity thickening* and *filtration*. Moreover, the concentration can be carried out by leaching in a heap or in a reactor; also mineral concentrates can be further handled by leaching. The main successive steps in the mineral processing sequence from the mine to the port or smelting are presented in Figure 1.

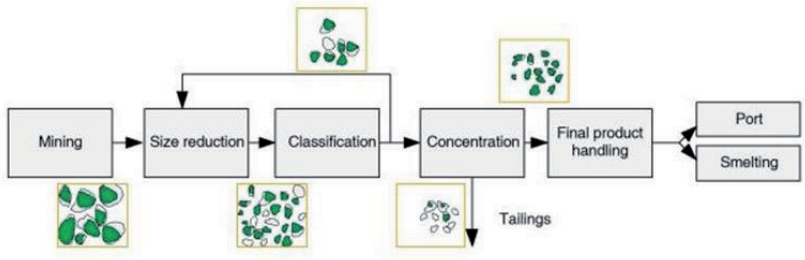

Figure 1. Main operation of a mineral processing plant (Sbárbaro and Villar (edit.), 2010).

In the following subsections the operation of the major process equipment utilized in the case processes of this thesis are described in general. In addition, a more detailed explanation of the process phenomena and modeling practices is given for the countercurrent dense medium separators (Floatex), the flotation cells and the gravity thickeners, since these models are applied more extensively in the case studies in Chapter 5.

In modeling of mineral benefication the model type can vary largely based on usage. For process control purposes data based models can be highly suitable. However, for process audits and studies of unit operations for a certain ore processing and operating conditions, mineralogical information should be incorporated into the model. This type of model can be said to be a *property based model*, where the material is treated based on its physical and chemical properties (Lamberg, 2010). The model should be based on known mineral composition, particle size classes, particles with defined properties (e.g. Satmagan value defining proportion of magnetic compounds), possibly mineral liberation analyzes, etc. Especially in flotation the property based model relies on floatability component model having different kinetic types – fast floating, slow floating and non-floating – for each mineral. The kinetic parameters should be preferably determined based on laboratory flotation test. Recently, the link between floatability components and particle physical characteristics has been studied by Welsby et al. (2010).

2.1 Grinding Mills

The size of the crushed ore is further reduced by applying impact and abrasion forces, typically in tumbling mills. The purpose of the size reduction prior to concentration is to liberate the valuable minerals by continuing the breakage to the fineness of the mineral grain size. Also, the size reduction prepares the particles to be suitable size for the downstream processes, for example for flotation or pelletizing. The natural grain size of the same mineral in different ores can vary widely and over-grinding of the valuables should be avoided (Lynch, 1977). Therefore, the grinding circuits can also incorporate concentration equipment in order to remove certain particles at an early stage.

Grinding mills can be classified into *tumbling* and *stirred* mill types, according to how the charge motion is generated (Wills and Napier-Munn, 2006). Common tumbling mill types in mineral processing, in terms of the grinding media, are: *rod mills*, *ball mills*, *autogenous mills* (AG), and *semi-autogenous mills* (SAG). If hard screened ore particles are used as the grinding medium together with steel balls, the mill is called a *pebble mill*. Figure 2 presents a diagram of material flow through an overflow mill. In addition to the grinding media, the design of the mills varies in terms of the lifter shape inside the mill wall, and in the case of grate discharge mills, different grate and pulp lifter options. Moreover, a mill can be equipped with a trommel screen after the discharge trunnion.

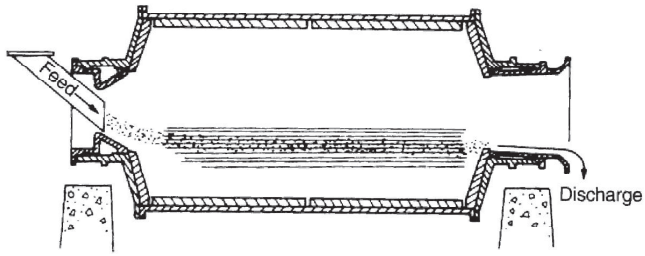

Figure 2. Schematic figure of overflow rod mill (Wills and Napier-Munn 2006).

Grinding is the most energy-intensive mineral processing unit operation. Several formulas for predicting the mill power draw exits. Brochot et al. (2006) have presented equations used in a comminution modeling software package called *USIM PAC*. It provides models for rod-, ball-, SAG- and pebble mills. They incorporate parameters of mill dimensions, mill rotation speed, mill loading fraction, fraction of grinding media and properties of the solids in the mill. Similar parameterization for tumbling mills is utilized also in Napier-Munn et al. (2005), where calculation of the mill gross power is divided into no-load power and net power drawn by the charge. For rod mills King (2001) has presented a power draw formula incorporating a fraction of the mill volume loaded with rods, mill diameter and mill rotation speed.

The energy requirement increases when the size reduction is continued towards a still a finer product. Early modeling practices of the comminution were formulated in the 19th century in the *Kick* and *Rittinger laws*, and later on in the 20th century in the *Bond law*, relating the applied energy and achieved breakage, in terms of change in a certain particle size class or passing size. Nowadays, modeling of the comminution can be categorized into the fundamental and black box models. Fundamental models incorporate laws of motion of the each single particle, utilizing discrete element method (DEM) computation. The method is computationally intensive; modeled contacts between the particles typically yield impact and abrasion/attrition energy distributions over a certain period of milling. An example in Figure 3 visualizes a result of a DEM simulation.

Fundamental comminution modeling is computationally intensive, which is still limiting the use of it, especially with large-scale simulations (over 100 000 particles) involving small particle sizes (Wills and Napier-Munn, 2006). Recently, research efforts have focused on combining the simulated energy distributions and the resulting breakage. Datta and Rajamani (2002) proposed the use of population balance modeling, whereas Morrison et al. (2006) compared the DEM simulated and the laboratory mill charge motions and the rock wear rates. Powell and McBride (2006) described two

modeling schemes: (i) the use of the energy distributions after the simulation or (ii) modeling the particle breakage progeny during the simulation. Further, Powell et al. (2008) have discussed a unified comminution modeling scheme and addressed the key areas still needing development. Recently, Tuzcu and Rajamani (2011) have combined the DEM impact spectra based selection function into the population balance model to predict the resulting particle size distribution. The model was verified experimentally with a laboratory batch mill. The authors stated that the industrial SAG mills can also be modeled in a similar manner based on the drop-weight rock tests.

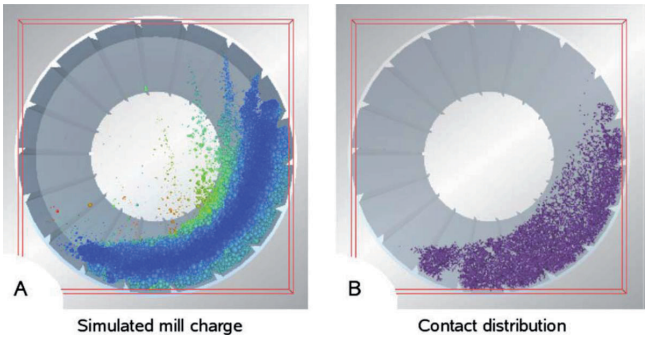

Figure 3. A) Motion of 11 400 particles in Discrete element simulation of a mill B) contact events during the same time instant of the simulation (Powell and McBride, 2006).

Black-box modeling of the grinding mills is well suited to flowsheet wide modeling; early simulation work carried out with several mill types and circuit configurations can be found in Lynch (1977). Commonly, the calculation of the mill outlet particle size distribution is presented in the following matrix form, with a *breakage function* B_{br} and a *selection function* S. The breakage function is a vector defining the distribution of the material after an occurrence of the primary breakage; on the other hand the selection function defines the probability of the breakage rate in a size class. Thus the formula becomes,

$$p = B_{br} \cdot S \cdot f + (1 - S) \cdot f, \qquad (1)$$

where p and f are product and feed particle size distributions. For ball milling, two commonly applied variations of the model exist: the *population balance model*, with a definition of the solids residence time, and the *Whiten perfect mixing model*, utilizing ratio of the rate of breakage and the discharge rate, which can be estimated from the actual feed and product measurements. In the case of AG and SAG mills, a more detailed laboratory breakage and abrasion test is needed in order to define the

breakage appearance (term for the selection probability in the Whiten model context). Also, semi-empirical mill outlet flow rate functions for grate end mills exist. The grinding mill power draw for a certain ore type is related both to the throughput and fineness of the feed and the product. It can be predicted and implemented in simulations with Bond operating work index *WIo* (kWh/t) as applied later in Eq. (56). (Lynch, 1977; Prasher, 1987; King, 2001; Napier-Munn et al., 2005; Wills and Napier-Munn, 2006)

In this thesis the grinding mills are present in all of the case plants. The Kemi grinding-gravity separation monitoring is described in Section 5.3 and the grinding circuit control experiments in Section 5.4. In addition, the Pyhäsalmi grinding-flotation simulation study and the model-based control of the Siilinjärvi grinding circuit are described in Section 5.4.

2.2 Floatex Density Separators

A Floatex density separator can be utilized for the size separation and the concentration duties. A Floatex density separator (FSD) is a hydraulic classifier, based on a *hindered settling* of particles in conjunction with a countercurrent upward *teeter water* flow. The slurry and water form together an autogenous fluidized dense medium bed with a certain density and pressure. A simplified structure of the FSD indicating the directions of the feed-, over- and underflows and the teeter water feed pipelines throughout the cross section is shown in Figure 4. It has been reported that in the case of a multi component feed (fine coal), having both particle size and density distribution, at low pressures the FSD acted primarily as a size separator, whereas with higher bed pressures it was more effective as a concentrator, due to proper development of suspension density (Sarkar, at al., 2008; Sarkar and Das, 2010).

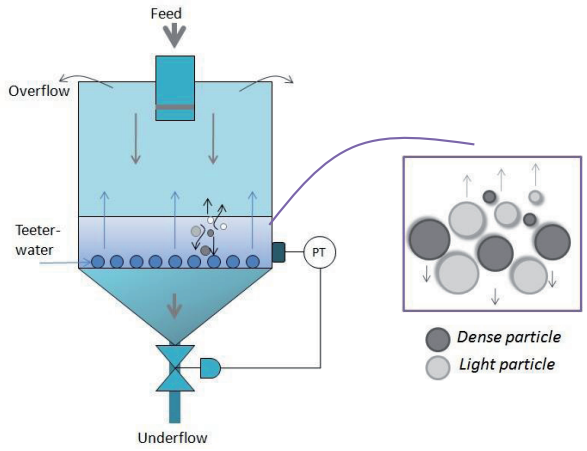

Figure 4. Flow directions in a Floatex density separator with a bed pressure control, and an illustration of size and density based separation of the particles in the fluidized bed.

Particle motion in a Floatex density separator is a complex combination of the fluid-particle and particle-particle interactions, especially when inhomogenity of the raw material exists. To simplify the modeling, a steady-state force balance can be considered. In hindered fluidized settling a particle experiences *buyoyant*, *drag* and *gravitation* forces (Felice, 1995). All these will determine the *terminal settling velocity* of the particle. Separation of the particles takes place in a dense medium bed, established with the upward flowing teeter water. The velocity of the particle relative to the liquid, called the *slip velocity*, determines whether the particle reports to the overflow or underflow stream.

Several equations for calculating the slip velocity have been proposed by various authors over relatively long period of time. Galvin et al. (1999a) presented an equation, modified from the Richardson-Zaki formula, covering also suspensions containing both particles of different sizes and densities. The proposed equation has been also concluded to have the best performance in an experimental test when compared with three other commonly available calculation formulas (Das and Sarkar, 2010). The slip velocity of the size fraction i and density j, V_{ij} (m/s) is a function of particle terminal settling velocity $U_{t,ij}$ (m/s) and the composition of the suspension as follows (Galvin, et al., 1999a)

$$V_{ij} = U_{t,ij}\left(\frac{\rho_{ij}-\rho_{sus}}{\rho_{ij}-\rho_{water}}\right)^{n_{ij}-1}, \qquad (2)$$

where ρ_{ij} (kg/m³) is the density of the particle, ρ_{sus} (kg/m³) is an average density of the suspension, ρ_{water} (kg/m³) is the density of the fluidization

water and n_{ij} is a dimensionless Richardson-Zaki index. The average suspension density ρ_{sus} (kg/m^3) can be obtained from the measured pressure P_m (kPa) and the pressure of water filled separator $P_{waterbed}$ (kPa) with

$$\rho_{sus} = \frac{P_m}{P_{waterbed}} \rho_{water}. \quad (3)$$

The Richardson-Zaki index n_{ij} is a function of dimensionless particle Reynolds number Re_t, and again, several formulas for calculation of that exist. However, a logistic curve proposed by Rowe (1987), is claimed to be more accurate than another commonly used Graside Al-Dibouni formula (Das, et al., 2009). The index is obtained with

$$n_{ij} = \frac{2\left(2.35 + 0.175 Re_t^{0.75}\right)}{\left(1 + 0.175 Re_t^{0.75}\right)}. \quad (4)$$

Terminal settling velocity $U_{t,ij}$ (m/s), used in (1), can be obtained for spherical particles from the definition of the particle Reynolds number Re_t (in the terminal settling velocity), see, for example, McCabe et al. (1993), resulting in

$$U_{t,ij} = \frac{Re_t \mu_{water}}{d_p \rho_{water}}, \quad (5)$$

where μ_{water} (Pa·s) and ρ_{water} (kg/m^3) are the fluidization water viscosity and the density respectively and d_p (m) is the particle diameter. Finally, the Reynolds number of a particle is calculated with an empirical correlation. A correlation proposed by Hartman et al. (1989) is claimed to predict the terminal settling velocity with ±1 % estimation error, and is thus more accurate than another commonly used Zigrand and Sylvester (1981) correlation, used, for instance, in Galvin et al. (1999b). Moreover the Hartman correlation is claimed to be independent of the settling regime. The calculation procedure for the Reynolds number is (Hartman et al., 1989):

$$log_{10} Re_t = P(A) + log_{10} R(A) \quad (6)$$

$$P(A) = [(0.0017795A - 0.0573)A + 1.0315]A - 1.26222 \quad (7)$$

$$R(A) = 0.99947 + 0.01853\sin(1.848A - 3.14) \quad (8)$$

$$A = log_{10}Ar, \quad (9)$$

where Ar is the dimensionless Archimedes number, which is calculated using the acceleration due gravity g (m/s²) and the properties of the liquid and the particle with the above notations:

$$Ar = \frac{d_p^3 g \rho_{water}(\rho_{ij} - \rho_{water})}{\mu_{water}^2}. \quad (10)$$

If the particles in the feed material are nonspherical, the equation (5) is not valid for calculation of the terminal settling velocity. Chhabra et al. (1999) have compared several available *drag coefficient* calculation methods for nonspherical particles. A formula by Chien has a relatively simple form for the drag coefficient $C_{D,ij}$, using the particle Reynolds number at terminal settling velocity Re_t and particle sphericity ψ as parameters:

$$C_{D,ij} = \frac{30}{Re_t} + 67.289exp(-5.03\psi). \quad (11)$$

The definition for the sphericity ψ is: surface area of a sphere of volume equals the particle divided by surface area of the particle. The values of the sphericity (or shape factor) vary from 0.1 ... 1 (disc to sphere); for example, the sphericity of a cube is $\psi = 0.806$. It should be noted, when applying equation (11) to the particle size classes, that equal volume sphere diameters for calculation of Re_t and corresponding $C_{D,ij}$ are also used.

The grad coefficient equation (11) is applicable in the ranges $0.2 \leq \psi \leq 1$ and $Re_t < \sim 5000$. Also another formulation by Hartman et al. (1994) uses directly the sphericity factor for the drag coefficient calculation; however the validity range of the sphericities is narrower ($0.67 < \psi$). In comparison with other methods, where a wide database of particle properties from literature was used, Chien's method gave fairly good overall results; the maximum error occurred in the case of cone shaped particles (Chhabra, et al., 1999). For the spherical particles, equation (11) overpredicts the drag

coefficients. Thus for spheres, Eq. (5) should be used for the calculation of the terminal settling velocity instead. However, the drag coefficients with various non-unity sphericity factors calculated using Eq. (11) are well consistent with the graphical chart, presented in Rhodes (1998).

For non-spherical particles the terminal settling velocity $U_{t,ij}$ (m/s) is finally obtained from the drag coefficient with a formula using the above notations, derived, for example, in Heiskanen (1993)

$$U_{t,ij} = \sqrt{\frac{4d_p\rho_{ij}\left(\rho_{ij} - \rho_{water}\right)/\rho_{water}}{3C_{D,ij}}}. \quad (12)$$

Next, when the particle slip velocity is obtained by using Eq. (2), it is compared with the *interstitial teeter water velocity*. Particles having lower slip velocity than the interstitial teeter water velocity, report to the overflow stream. The separation efficiency depends on the average poroucity of the medium, called voidage ε_{avg}, which is calculated using the average density of the particles $\rho_{avg.particle}$ (kg/m^3), suspension density ρ_{sus} (kg/m^3) and the water density ρ_{water} (kg/m^3) (Das, et al., 2009)

$$\varepsilon_{avg} = \frac{\rho_{avg.particle} - \rho_{sus}}{\rho_{avg.particle} - \rho_{water}}. \quad (13)$$

From the superficial teeter water velocity (m/s)

$$v_{teeter.sup} = \frac{F_{teeter}}{A_{floatex}}, \quad (14)$$

the interstitial teeter water velocity (m/s) is then obtained

$$v_{teeter.int} = \frac{v_{teeter.sup}}{\varepsilon_{avg}}. \quad (15)$$

Moreover a mass balance over the Floatex is written as

$$Ff_{ij} = Uu_{ij} + Oo_{ij} \quad (16)$$

$$F = U + O, \quad (17)$$

where F is the feed mass flow rate (t/h), U (t/h) is the underflow mass flow rate, O (t/h) is the overflow mass flow rate, f_{ij}, u_{ij} and o_{ij} are density by size mass compositions of the respective streams.

The above equations (2) – (17) describe the computational separation of the feed mass flow to the overflow and underflow streams of the Floatex apparatus. Thereby they determine the cut size of the separation d_{50} (m). However, this is still inadequate in order to compute detailed overflow- and underflow stream compositions. To take into account the random movement of the particles, a separation efficiency curve is fitted to the pre-determined cut size. Here, the separation efficiency y'_p is obtained from Venkoba Rao, et al. (2003). When written to fit the cut-size point the separation efficiency y'_p has the form

$$y'_p = 0.5\left[1 + erf\left(Ad^c_{p,ij}\left(\rho_{ij} - \rho_f\right) - B\right)\right], \qquad (18)$$

where *erf* is the well-known error function (a sigmoid shape function obtained from Gaussian distribution), ρ_{ij} (kg/m3) is the density of the solids, ρ_f (kg/m3) is the density of the total feed flow, $d_{p,ij}$ (m) is the particle mean size in the size class and c is an adjustable parameter. Thus formula (18) presents the size-density partition curve (or surface) relying on a stochastic Gaussian zero mean random variability of the particle velocity. It incorporates a settling velocity formula, yielding to the form (yp'), where the variance and other constants are lumped into parameters A and B. The parameters A and B are obtained from the calculated teeter interstitial velocity Eq. (15), standard deviation of the particle slip velocity $\sigma_{v,slip}$ (m/s), which is a mineral specific adjustable parameter, and from the pre-calculated cut-size d_{50} (m) by the applying formula (Venkoba Rao, et al., 2003)

$$B = \frac{v_{teeter.int}}{\sigma_{v,slip}\sqrt{2}} \qquad (19)$$

and, when the particle settling velocity and fluid drift velocity are equal at the cut-size point, the parameter A can be derived from (Venkoba Rao, et al., 2003)

$$A = \frac{B}{\left(\rho_{ij} - \rho_f\right)d^c_{50}}. \qquad (20)$$

It can be noted that the effect of the particle density and the feed density cancels out in Eq. (18). The parameters A, B and c together capture the random particle motion effects. Roughly, parameter A accounts for the viscous forces, B for the fluid drift and c for the hydrodynamic conditions and turbulence (Venkoba Rao, et al. 2003; Venkoba Rao and Kapur, 2008).

The procedure for applying the phenomenological equations of the Floatex density separation (FSD) to obtain the cut-size of each mineralogical species in the system and accomplishing the separation modeling with a separation efficiency dictated by the particle random motion yields the *corrected efficiency curve* or the *corrected Tromp curve*. Similarly, the calculated cut-size refers to the corrected cut-size, which is also typically used in design and scale up of classifiers (Heiskanen, 2003).

In addition, when taking into account the bypass portion of the fine end of the distribution, the *uncorrected efficiency curve* y_p is obtained (Wills and Napier-Munn, 2006):

$$y_p = y_p'(1 - r) + r, \qquad (21)$$

where r is the part of the fine end lost into the underflow stream, carried by the water flow. The cut-size, called the *Tromp partition index*, resulting from Eq. (21) is finer than the cut-size of Eq. (18).

In this thesis the Floatex density separators are modeled and studied in the Pyhäsalmi pilot equipment case and with the Siilinjärvi process data in Section 5.2.2. The model equations (2) - (21) describing the separation phenomena are utilized in the studies.

2.3 Flotation Cells

Froth flotation was patented back in 1906, since that time it has become the major mineral concentration technique. The concentration takes place in a solids-water-air –mixture, based on the different physico-chemical surface properties of the mineral particles. The solids transport from a *pulp phase* (called also a *collection zone*) to a *froth phase* has three major mechanisms: (i) selective *attachment* to air bubbles, referred to as *true flotation*; (ii) *entrainment* with water and; (iii) the physical *entrapment* (or aggregation) of the particles.

The most common practice is to recover the valuable mineral into the froth phase in *direct flotation*; oppositely, in *reverse flotation* the gangue material is separated into the froth. The selective separation of different mineral particles with true flotation is achieved based on the differences in hydrophobicity of them. Thus, a mineral can be categorized into either *polar* or *non-polar* type; the latter being hydrophobic and having a naturally high floatability. Anyhow, the kinetic characteristics of minerals are practically always affected by the treatment of flotation reagents. *Collectors* adsorb, during the required conditioning time, to the surface of a particle, making it hydrophobic and thus more likely to attach to an air bubble. *Regulators* include *activators* and *depressants*, affecting the attachment of certain minerals to the air, the regulators are also used for the pH control of the pulp. *Frothers* are added to create a stable enough froth phase.

In addition to the reagent dosage, the most important control variables of a flotation cell are the pulp level, having impact on the froth height and the air feed rate; also, in some cases, the impeller speed can be controlled. The volume of the flotation cells in new installations can be more than 200 m^3, since the relative investment costs and operating costs decrease with increasing cell size (Allenius et al., 2008). An example of a typical industrial flotation cell is shown in Figure 5.

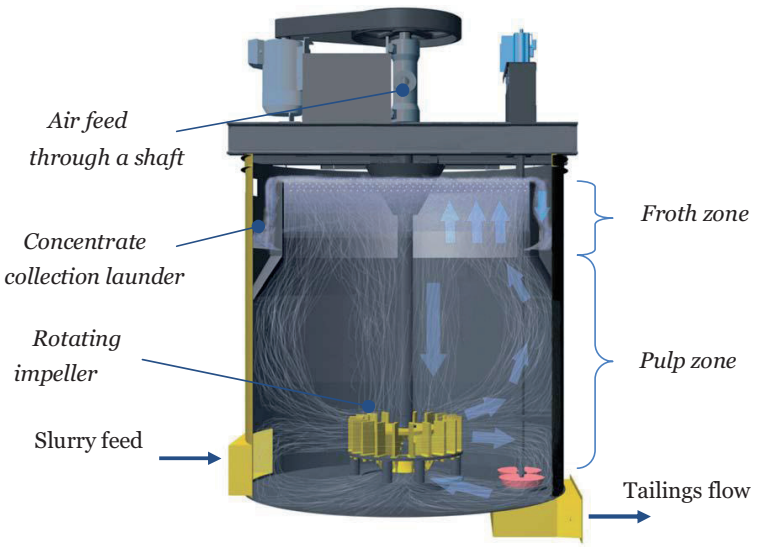

Figure 5. Example of an industrial flotation cell with indication of main components. (CAD image: courtesy of Outotec Minerals Oy)

Flotation remains partly poorly understood phenomenon, and modeling of that for the simulation and scale-up purposes largely relies on semi-empirical correlations. Modeling can be divided into the pulp zone and the

froth zone models (see Figure 5). In addition to them, a concept of the quiescent zone, which is less turbulent, but still provides perfect mixing of the water and the fine particles, can be distinguished between the pulp and the froth zones (Savassi, 2005).

The floatability of material is related to the kinetic characteristic of that and thus forms the basis for the pulp zone modeling. When modeling the froth zone, the entrainment, drainage and froth recovery can be treated separately. The key machine operating parameters are the superficial gas velocity J_g (m/s) and the bubble surface area flux S_b (1/s). The superficial gas velocity can be estimated by using the volumetric air flowrate to the cell Q_{AIR}(m³/s) and the cross sectional area of the cell A_{cell} (m²) (Gorain et al., 1999; Alexander et al., 2003)

$$J_g = \frac{Q_{AIR}}{A_{cell}}. \tag{22}$$

The superficial gas velocity can vary across the cell area as verified with a measurement probe in Gorain et al. (1996). The variation is most probably related to an uneven air bubble size distribution and gas hold up variations across the cell area, as measured in similar conditions by Gorain et al. (1995a and 1995b).

It has been shown by industrial measurements in Dahlke et al. (2005) that a cell gas holdup is a linear function of gas velocity J_g in normal operating range (ca. $0.5 < J_g < 2.5$ cm/s). The gas holdup affected by the cell meachanism, but also by slurry properties and chemistry, particularly frother dosage. Both the frother dosage and the superficial gas velocity have been shown to have an impact on the air bubble size; also industrially fitted functions are presented in Nesset et al. (2006). Air bubble size as a function of frothers, and determination of the critical coalescence concentration (CCC), as well as the J_g – bubble size relationship has been studied in Grau et al. (2005).

The bubble surface area flux S_b (1/s) describes the available air bubble surface area per unit of the cell cross-sectional area. If the superficial gas velocity J_g (m/s) and the bubble size d_b(m) are known, S_b can be calculated using (Wills and Napier-Munn, 2006)

$$S_b = \frac{6J_g}{d_b} \tag{23}$$

To predict the bubble surface area flux under different operating conditions of industrial scale flotation, the following correlation has been proposed by Gorain et al. (1999)

$$S_b = 123 N_s^{0.75} J_g^{0.44} A_s^{-0.10} P_{80}^{-0.42}, \qquad (24)$$

where N_s is the impeller peripheral speed (m/s), J_g is the superficial gas velocity (cm/s) calculated using Eq. (22), A_s is the aspect ratio of the impeller and P_{80} is the 80% passing size (μm) of the slurry solids. The parameters were fitted based on 100 data sets. The authors also presented a slightly different parameterization based on another validation data, including also cases with self-induced air impellers. It was suggested that Eq. (24) could be improved by including the slurry viscosity instead of the particle size. As a limitation, model (24) was stated to overestimate values of S_b when flooding ('boiling' of the air bubbles) due to high J_g or if high turbulence prevents the bubble size to decrease due to high N_s velocities.

The kinetic rate constant of flotation k (1/s) has been experimentally tested to have a linear relationship at shallow froth depths with dimensionless ore specific floatability P, the bubble surface area flux S_b(1/s) and the froth recovery R_f (Gorain et al., 1998)

$$k = P S_b R_f. \qquad (25)$$

Still, at intermediate and deep froth layers some non-linearity exists. Gorain et al. (1998) claimed that the relationship between k and S_b should be independent of the impeller type. Later on, Heiskanen (2000) demonstrated the impact of the gas dispersion efficiency and thus the effect of the impeller types. He also pointed out that the rate constant starts decreasing for coarse particles at high superficial gas rates, as experienced in industry.

The froth recovery R_f can be estimated by varying the froth depth of a cell. Linear extrapolation of the rate constant to the froth depth of zero yields the collection zone rate constant k_c (1/s) and thus the following relationship (Alexander et al., 2003)

$$R_f = \frac{k}{k_c}. \qquad (26)$$

In addition, recovery due to the true flotation R_T is obtained, when perfect mixing of the pulp zone is assumed, as

$$R_T = \frac{k_c \tau}{1 + k_c \tau}, \quad (27)$$

where τ (s) is the cell pulp zone residence time. In dynamic simulation applications the simulation time step is multiplied with the flotation rate constant and current mass of the mineral in the cell, yielding the concentrate mass flow rate, thus indirectly the recovery of the particles in that time span is obtained (Lamberg et al, 2009).

The true flotation and froth recovery do not merely describe the overall flotation recovery. For the particles of sizes less than 50 μm the entrainment phenomenon starts to be a significant factor (Wills and Napier-Munn, 2006). The entrainment factor *Ent* (normally between 0…1) is defined as a ratio of the entrained particles to the concentrate to the mass transfer of water to the concentrate. Recovery of solids due to the entrainment R_E is calculated linearly from the water recovery R_w:

$$R_E = Ent \cdot R_w. \quad (28)$$

Moreover, recently Zheng et al. (2006b) have concluded that the above relationship is close to linear especially for the fines, based on industrial scale test work. To estimate the entrainment recovery R_E Savassi et al. (1998) have presented an empirical partition curve, that expresses the entrainment *Ent* in terms of a particle cut size having 20% entrainment ξ (μm) and a drainage parameter δ, describing the drainage of coarse particles. The entrainment Ent_i for each particle size class d_i (μm) can be calculated using the formula

$$Ent_i = \frac{2}{exp\left(2.292\left(\frac{d_i}{\xi}\right)^{adj}\right) + exp\left(-2.292\left(\frac{d_i}{\xi}\right)^{adj}\right)}, \quad (29)$$

where the drainage is impacting by means of an adjustment parameter,

$$adj = 1 + \frac{ln(\delta)}{exp\left(\frac{d_i}{\xi}\right)}. \quad (30)$$

The parameters ξ and δ are to be correlated (linearly) with the air residence time in the froth phase λ_{air} (s), which depends on the froth height H_f (m) and the superficial gas velocity J_g (m/s):

$$\lambda_{air} = \frac{H_f}{J_g}. \tag{31}$$

Elsewhere, Yianatos and Contreras (2010) have also presented an empirical entrainment factor model, where they have parameterized the model with the particle size and the drainage term. To estimate the water recovery R_w as a decreasing function of the air residence time λ_{air}, the following equation was applied by Savassi et al. (1998) with experimentally fitted parameters a and b

$$R_w = a\lambda_{air}^b. \tag{32}$$

Finally, calculation of the overall recovery, incorporating both the true flotation, froth recovery and the entrainment terms, can be written (Savassi, 2005)

$$R = \frac{k_c \tau R_f (1 - R_w) + Ent R_w}{\left(1 + k_c \tau R_f\right)(1 - R_w) + Ent R_w}. \tag{33}$$

Recently, the froth recovery, the water recovery and the entrainment have been observed to be related to the amount of air recovered over the cell lip to the concentrate. The air recovery α can be calculated based on the froth image analysis by using the froth velocity v_l(m/s) and depth of the froth over the launder lip h (m) with the lip length l_l (m) and the air feed rate (m^3/s) (Neethling and Cilliers, 2008)

$$\alpha = \frac{v_l h l_l}{Q_{AIR}}. \tag{34}$$

The air recovery can be also determined based on image analysis of bubble collapse rate and the mean size of the bubbles. Estrada-Ruiz and Pérez-Garibay (2009) used this method to compare different air recovery models; they also proposed a semi-phenomenological model, based on volumetric flow rates and bubble diameter. For simulator usage, an equation where the air recovery is linearly dependent on the froth height H_f

(m) and maximum froth height $H_{f,max}$ (m), where the all bubbles are bursting, is convenient (Zheng et al., 2006a)

$$\alpha = 1 - \frac{H_f}{H_{f,max}}. \tag{35}$$

It has been shown that the air recovery has a maximum as the air rate is increased (Neethling and Cilliers, 2008). Also, the air recovery parameter α can be used to predict the entrainment parameter Ent_i of different particle sizes with a theoretical formula based on the particle settling velocities presented by Neethling and Cilliers (2009). The formula takes into account the superficial gas velocity and the froth height as cell operating parameters. Neethling and Cilliers (2003) have also given a theoretical model for the concentrate water flow rate calculation, based on the measurement or estimation of the air recovery, the froth bubble size and the superficial gas velocity. The model was compared with other water recovery formulas, and judged to be well suited for practical process control purposes (Zheng et al., 2006a).

Later on, for the water recovery model by Neethling et al. (2003), Smith and Cilliers (2010) have presented experimental parameter estimation based on rougher bank tests. For the froth recovery, Neethling (2008) has presented a theoretical model, based on gas rate, air recovery and the change of the bubble size across the froth layer. The model takes into account different particle sizes, having different settling velocities in the Plateau borders of the foam after a detachment of a particle from a bubble has occurred. It has been shown that the air recovery has a maximum value (peak air recovery, PAR), where also the maximum recovery of the valuable mineral occurs; this has been utilized successfully in flotation bank air profile optimization in Smith et al (2008) and Smith et al. (2010).

When applying formulas involving the bubble size information provided by image analysis segmentation, the averaging method in calculation of the mean bubble size should be considered properly. The size estimation mismatches have been demonstrated with the Pyhäsalmi Mine rougher flotation test data in Neethling et al. (2003). Later on, a simulation case in a South African platinum mine showed that the largest error source originate from the estimation of the overflowing average bubble size (Smith et al, 2008). In addition, it was remarked that the foam surface bubble size, measured using image analysis, is not the same as the lip overflowing size, and certain transformation calculus should be carried out.

In this thesis the flotation processes are present in the control simulation studies. Section 5.4.1 includes flotation simulation experiments with different control setups and a control study of a grinding-flotation process chain case. Especially, the flotation model equations (22) - (35) are utilized as part of the process simulator used in the analysis of froth velocity control benefits.

2.4 Gravity Concentration with Spirals and Reichert Cones

Generally, gravity concentration is sensitive to the presence of slimes (particle sizes less than around 10 μm), since it increases slurry viscosity, reducing the sharpness of the separation. Therefore, a common practice is thus to remove the slimes beforehand, for example with hydrocyclones. For the same reason the separation efficiency is sensitive to deviations from an optimal feed pulp density; which is therefore often a controlled variable. (Wills and Napier-Munn, 2006)

Separation in Reichert cone units takes place in pinched sluices. Reichert cones are most efficient in the 100...600 μm particle size range (Wills and Napier-Munn, 2006). The feed slurry is distributed evenly, using the upper cone surface, down to a center toward cone. The thickness of the slurry bed increases from the cone periphery (diameter Ø typically 2 m) to the concentrate drawoff slot around four times (Burt, 1984). Meanwhile, the particles form a stratified layer, where the high specific gravity minerals are placed near the concentrating surface. The concentrate is collected with a vertically adjustable slot mechanism, while the lighter particles pass over the gap heading to a tails pipe in the cone center. The Reichert cone can be structured as a single or double cone assembly. A schematic figure of the cone structures are shown in Figure 6a.

Spiral concentrators – sometimes called Humphrey's spirals according to the original inventor of them – are helical downwards conduits with ports for concentrate removal. The particle size range of an efficient separation with the spirals vary between 50...1000 μm, depending on the device type (Burt, 1984). Nowadays, a wide range of different device constructions are available. An additional wash-water can be fed from the inner radius, carrying lighter particles to the outer edge of the spiral. However, recent developments in spiral technology have been wash waterless operation, having adjustable splitter ports at the bottom of the spiral. Figure 6b illustrates the separation of the low and high density particles to the tailing-, middling- and concentrate streams. (Wills and Napier-Munn, 2006)

a) REICHERT CONE b) SPIRAL

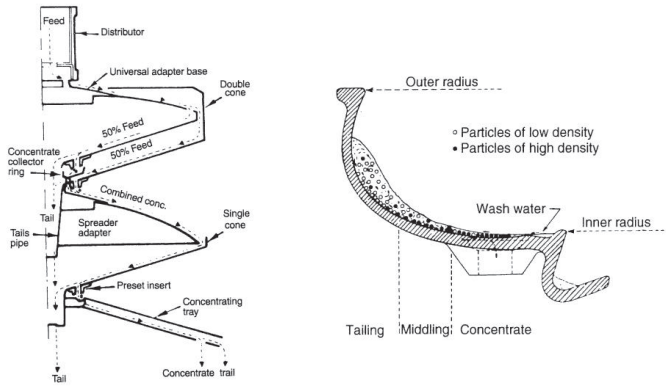

Figure 6. Schematic cross-section figures of a) Reichert cone and b) spiral gravity separators (Wills and Napier-Munn, 2006).

Modeling of the particle separation in Reichert cones is based on potential energy variations, when particles of different densities change (vertically) places in a settled bed. This causes a *stratification flux*, which has an opposite *diffusive flux* caused by a random particle-particle and particle-fluid interaction. In addition, experimental concentrate flowrate vs. feedrate slopes need to be defined by adjusting the slot settings. Equations describing the fluxes are solved in a dynamic equilibrium and the resulting stratified bed is split to match the experimental gap take-off flowrate, in order to calculate the compositions of the discharge streams of the cone. The calculation procedure with good experimental results is presented in King (2001). The method is further extended to incorporate the effect of particle size distribution, in addition to density/grade distribution, by Venkoba Rao (2007).

Particle separation in spirals is based on a combination of the centrifugal and shear forces, hindered settling of the particles and the effect of interstitial trickling through the flowing particle bed (Burt, 1984; Wills and Napier-Munn, 2006). Holland-Batt (1989) has presented a semi-empirical procedure describing the calculation of slurry velocity components of downward and across the spiral through directions. The calculation utilizes the Manning equation for open channel flow velocities and a free vortex equation for the across spiral velocities. The calculated particle velocities were further used to predict the cut sizes and solids distributions of the streams. Later on the calculation was expanded also to take into account the shear forces in more details; the obtained predictions were compared experimentally by various authors (Loveday and Cilliers, (1994); Atasoy and Spottiswood, 1995, Holland-Batt, 2009).

In this thesis the process data applied for the plant-wide predictive modeling in Section 5.3 is obtained from a gravity separation process of the Kemi concentrator. The process includes both Reichert cone separators followed by subsequent spiral separators.

2.5 Gravity Thickeners

Gravity thickeners are used for continuous slurry sedimentation on an industrial scale. The equipment is a relatively simple, large shallow tank (Ø varying from 2 to 200 m) with slow rotating radial rake arms, shown in Figure 7. The feed slurry flows downward until the zone of equal density, where it continues moving radially outwards at a decreasing velocity. Gradually the flow separates to downward flowing suspension and to upward flowing water being nearly free of solids. Vertical segments in the thickener can be categorized into the *clarification* zone above the feed level, the zone of the *hindered settling* and the *compression* zone near the bottom. Thick slurry is removed from the tank via an underflow cone with a sludge pump; the clarified water overflows to a weir. The sedimentation is usually boosted with *coagulation* and *flocculation* chemicals fed into the feed well. Coagulation chemicals bind together colloidal fine particles while flocculation is responsible for formation of more open agglomerates, where the reagent acts as a bridge between the particles. (McCabe, et al., 1993; Wills and Napier-Munn, 2006)

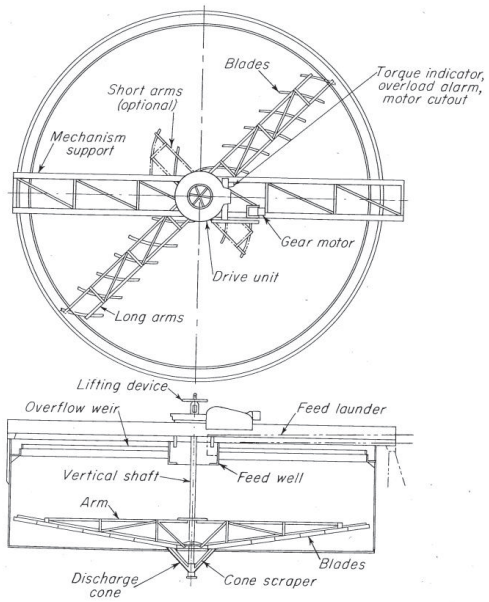

Figure 7. Construction of a gravity thickener (McCabe et al., 1993 / Eimco Corp.).

In control of the thickeners the underflow density is often the most important performance criterion. The control scheme includes: regulation of the reagents addition, regulation of the underflow withdrawal and the rake drive controls with a rising mechanism. In addition to conventional flow meters and slurry density sensors, a thickener is often equipped with a sediment bed level sensor. Also a sludge bed pressure sensor at the bottom of the thickener can be effective for control purposes, indicating the mass of solids in the tank. (Perry and Green, 2008)

A common control strategy is to control the underflow slurry density by manipulating the underflow pump speed. The sediment bed can be controlled by adjusting the flocculation ratio; a higher flocculation rate compresses the bed height, which has been also experimentally verified by Johnston and Simic (1991). Subsequently, at the same feed rate, the changes in the sludge bed depth also affect the underflow density (Concha and Bürger, 2003).

Therefore, an alternative control strategy is to compensate for variations in the underflow concentration by adjusting the flocculant dosage, while the slurry bed level is maintained by adjusting the underflow rate (Perry and Green, 2008). However, in the (multivariable) control philosophy it is important to take into account strong interactions between variables and long time delays and dead times and the possibility that the actual system response can be somewhat abnormal. For example, excessive flocculant addition may lead to, instead of increased underflow density, increased rake torque and disturbed operation that might require corrective action for several hours (Perry and Green, 2008).

A rapid rise in the rake torque can originate from several different reasons. Increased torque can result if the material in the thickener accumulates faster than it is removed. This situation can arise when considerable amount of coarse fraction occur in the feed. Then the coarse solids can separate from the pulp, causing difficulties in raking and pumping. The situation normalizes – in addition to raising the rakes – when the fine fraction of the feed slurry starts accumulating in the basin, enhancing buoyancy and fluidity and thus lowering the torque.

Another origin of the increased the torque, especially when the operating conditions remain unchanged, can be a formation of an *island*. The term means semisolidified mass accumulated in front of the rakes. The reason for the island formation is often an excessive use of flocculant, causing accumulation of a claylike consistent mass. This can be noticed from gradually increasing torque ending up in a torque spike. (Perry and Green, 2008)

Successful raking has an impact on the thickener overall operation and especially on even underflow density and flow rate. Over-raking causes back circulation in the outer parts of the thickener. On the other hand, insufficient raking increases the risk of rat-holing in the middle of the tank (Rudman, et al., 2008). In addition to the material transportation function, raking is the dominant mechanism in dewatering of the settled slurry, removing significantly intra-aggregate liquid (Farrow, et al., 2000). The raking efficiency has also been studied in Rudman et al. (2010); the ratio of the rake delivery and underflow rate was observed to be the key factor in the thickener operation and the underflow rate was suggested to be adjusted on a daily or hourly basis.

Modeling of a continuous thickener is based on a description of the total downward solids flux. The flux consists of the *transport flux* G_t where the solids are carried by the down flowing water and the *settling flux* G_s caused by particle settling through the water. The total flux G can be written (McCabe, et al., 1993)

$$G = G_t + G_s = u_f c_s + \left(\frac{dZ}{dt}\right) c_s, \qquad (36)$$

where c_s is the solids concentration, u_f is the downward fluid velocity, and $\frac{dZ}{dt}$ is the settling rate. The settling rate is determined by carrying out a batch settling test known as the *Kynch method*. A steady-state simulation practice based on the ideal Kynch model has been presented in King (2001).

In this thesis, the operation of an industrial concentrate thickener was monitored based on a simple dynamic mass balance calculation in conjunction with the mean density and the underflow cone pressure calculation formulas. In addition to the fresh concentrate slurry mass flow rate $\dot{m}_1$, the concentrate dewatering sections have often a back circulation flow $\dot{m}_2$ from the filtration stage to the thickener. When $\dot{m}_3$ is the underflow mass flow, the net mass accumulation is

$$\frac{dm_{solids}}{dt} = \dot{m}_1 + \dot{m}_2 - \dot{m}_3 . \qquad (37)$$

Next, the water mass is obtained, when the tank volume $V_{thickener}$ and solids specific mass ρ_{solids} are known, by

$$m_{water} = \left(V_{thickener} - \frac{m_{solids}}{\rho_{solids}} \right). \quad (38)$$

Water balance over the thickener can be written as follows:

$$\dot{v}_{overflow} = \dot{v}_1 + \dot{v}_2 - \dot{v}_3 + \dot{v}_{water\_addition}, \quad (39)$$

$$\dot{v}_{water,1} = \dot{v}_1 - \frac{\dot{m}_1}{\rho_{solids}}, \quad (40)$$

$$\dot{v}_{water,2} = \dot{v}_3 - \frac{\dot{m}_2}{\rho_{solids}}, \quad (41)$$

$$\dot{v}_{water,3} = \dot{v}_{water,1} + \dot{v}_{water,2} - \dot{v}_{overflow}, \quad (42)$$

where $\dot{v}_1$, $\dot{v}_2$ and $\dot{v}_3$ are the total volumetric flow rates of the two inflows and underflow respectively, $\dot{v}_{water,1}$, $\dot{v}_{water,2}$ and $\dot{v}_{water,3}$ are the volumetric water flow rates of them. Also, possible water addition to the underflow line $\dot{v}_{water\_addition}$ is taken into account. The overflow $\dot{v}_{overflow}$ water is calculated by assuming it to be clarified solids free liquid. Subsequently, the underflow mass flow rate is obtained with

$$\dot{m}_3 = (\dot{v}_3 - \dot{v}_{water,3}) \cdot \rho_{solids}. \quad (43)$$

Further, the thickener sludge average density is

$$\rho_{thickener} = \frac{m_{solids} + m_{water}}{V_{thickener}}. \quad (44)$$

Now, if the thickener is equipped with a pressure transmitter (in the underflow cone/line), also the calculated quantity of that can be obtained simply by

$$p_{underflow\_cone} = \rho_{thickener} \cdot g \cdot h_t, \quad (45)$$

where g is the acceleration due to gravity and h_t is the height of the slurry bed to the sensor.

In this thesis a gravity thickener is assessed by studying the process operation data and carrying out process experiments at the Siilinjärvi concentrator. The process monitoring system was constructed by applying equations (37) - (45) to estimate the mass balances over the equipment.

The system was implemented in the Siilinjärvi apatite concentrate thickener.

2.6 Particle Size Analyzers for Process Slurries

Particle size analysis of process slurry lines can be carried out with three application manners: at-line, on-line or in-line. In the at-line method the sample is transported to the laboratory for analysis; in the on-line method the analysis is performed automatically close to the process line; and in the in-line analysis the sample is kept in the process line during the whole sample preparation and measurement procedure. Common mineral particle size analysis methods includes: laser diffraction, image analysis, the acoustic (ultrasonic attenuation) method, the electric sensing zone method, gravitational sedimentation, sieving, elutriation methods (such as a cyclosizer) and the physical caliper positioning method. The results of different analysis methods are not directly comparable, since the particle properties, such as the shape factor, affect essentially the result. Currently, the most common on-line particle size analyzers apply the laser diffraction, ultrasonic or the movement of a physical caliber method. (Perry and Green, 2008; Wills and Napier-Munn, 2006; Napier-Munn et al., 2005)

Currently, for on-line analysis the most frequent measurement fractioning over the defined size distribution range can be obtained by the laser diffraction method. The method is based on a physical phenomenon where the particles of different sizes scatter the coherent light by certain size dependent angles. The principles for forming the diffraction patterns are illustrated in Figure 8. The spatial light distribution (Figure 8a) can be transformed to an angular distribution (Figure 8b) with a certain light intensity (Figure 8c). Currently two main algorithms, the Fraunhofer theory and the Lorenz-Mie theory, are available for calculation of the particle size distribution backwards from the measured intensity-angle pattern. The Mie theory is more computationally intensive but produces more accurate results especially for the sizes less than 50 μm. Moreover, the algorithm is applicable across the entire measurement range, and thus is a standard method in current laser diffraction analyzers. (Perry and Green, 2008; Jones, 2003)

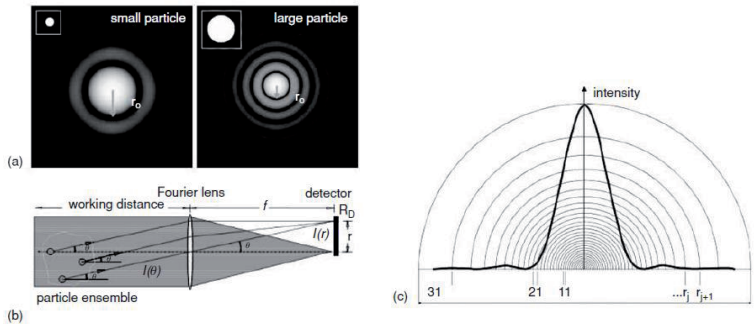

Figure 8. a) Diffraction pattern of laser light for small and large particle sizes, b) conversion of the angular distribution *I*(θ) to a spatial distribution *I*(r), c) intensity distribution of a a small particle on a photodetector (Perry and Green, 2008).

In this thesis the on-line particle size distribution analyses of the ground ore slurries are obtained based on the laser diffraction technique. Similar analysis equipment is utilized in all case plants, measuring the outlet slurries of the grinding circuits.

3 Brief Overview of Main Methods

This chapter describes the main methods used in the modeling and control studies of the case processes. Phenomenological modeling of the unit processes are described in Chapter 2. Here, the data-based PLS (*partial least squares*) modeling and its recursive updating technique is reviewed. Also, the two higher level process control methods, applied in this thesis, the *model predictive control* (MPC) and the *fuzzy control* are described. In addition, the *Kalman filtering* method used in a process monitoring application is shortly explained.

3.1 Partial Least Squares Modeling

The partial least squares (PLS) regression model is formed by constructing linear mapping between the m-couple of the *predicted variables* $\boldsymbol{Y}$ and the n-couple of the *predictor variables* $\boldsymbol{X}$, both having N rows of samples. Mapping of the variables is presented with the regression coefficient matrix $\boldsymbol{B}_{\mathrm{R}}$ $(n \times m)$ such that the estimates of the predicted variables $\hat{\boldsymbol{Y}}$ are composed

$$\hat{\boldsymbol{Y}} = \boldsymbol{B}_{\mathrm{R}}\boldsymbol{X}. \qquad (46)$$

A similar regression coefficient representation as in Eq. (46) is obtained also with the multivariate least squares regression technique, computed by means of the pseudoinverse formula

$$\boldsymbol{B}_{\mathrm{RLS}} = (\boldsymbol{X}^T\boldsymbol{X})^{-1}\boldsymbol{X}^T\boldsymbol{Y}, \qquad (47)$$

where $\boldsymbol{X}^T\boldsymbol{X}$ is the covariance matrix and $\boldsymbol{X}^T\boldsymbol{Y}$ is the cross-covariance matrix estimated from the sample data. However, the covariance of $\boldsymbol{X}$ may not be invertible, or the calculation can be numerically unstable if collinearity (rows are not linearly independent) exists, especially if the data is noisy. In the partial least squares (PLS) technique this issue is avoided. In the PLS method the input block is decomposed into a sum of the inner product of the *score* $\boldsymbol{t}$ and the *loading* $\boldsymbol{p}$ vectors, the corresponding matrices are $\boldsymbol{T}$ $(N \times l)$ and $\boldsymbol{P}$ $(n \times l)$

$$\boldsymbol{X} = \boldsymbol{t}_1\,\boldsymbol{p}_1^T + \boldsymbol{t}_2\,\boldsymbol{p}_2^T + \cdots + \boldsymbol{t}_l\,\boldsymbol{p}_l^T = \boldsymbol{T}\boldsymbol{P}^T. \qquad (48)$$

The original predictor data $\boldsymbol{X}$ is reduced and approximated in Eq. (48), by selecting the number of the *latent variables* less than the rank of the matrix $\boldsymbol{X}$: $l < d$. In addition, the loadings vectors are defined to be orthogonal, aligned into the directions of the largest variances in the original data. On the other hand, the scores $\boldsymbol{T}$ in Eq. (48) can be computed by multiplying the original data $\boldsymbol{X}$ with a weight matrix $\boldsymbol{W}^*$ $(n \times l)$

$$\boldsymbol{T} = \boldsymbol{X}\boldsymbol{W}^*. \tag{49}$$

Note that the above construction of the scores differs from the case of principal component decomposition, where the score vectors for a given data can be calculated using the loadings: $\boldsymbol{T} = \boldsymbol{X}\boldsymbol{P}$. In the same manner, as in Eq. (48), the predicted variables can be decomposed into "Y-scores" and the weights

$$\boldsymbol{Y} = \boldsymbol{U}\boldsymbol{C}^T. \tag{50}$$

Instead of the original data samples in $\boldsymbol{X}$ the scores $\boldsymbol{T}$ Eq. (49) are the predictors of $\boldsymbol{Y}$, thus Eq. (50) can be written

$$\boldsymbol{Y} = \boldsymbol{T}\boldsymbol{C}^T = \boldsymbol{X}\boldsymbol{W}^*\boldsymbol{C}^T. \tag{51}$$

The Equation (51) looks like a multivariate regression model (46), where the regression coefficient matrix is expressed as $\boldsymbol{B}_{\mathrm{R}} = \boldsymbol{W}^*\boldsymbol{C}^T$. Two main methods to calculate the PLS coefficients exist: NIPALS (*Non-Iterative Partial Least Squares*) and the kernel method; both having several modifications. In this thesis, the kernel-based recursive PLS algorithm, presented by Dayal and MacGregor (1997a), was applied. In the algorithm, the largest eigenvector of the product of the covariance matrices $\boldsymbol{Y}^T\boldsymbol{X}$ and $\boldsymbol{X}^T\boldsymbol{Y}$ is taken to obtain the first predictor weight vector $\boldsymbol{w}_1^*$. The computation proceeds by determining the weights of the predicted variables, and further deflating the covariance $\boldsymbol{X}^T\boldsymbol{Y}$ by subtracting the effect of the latent vector direction. This is repeated up to the number of the PLS latent variables. A more detailed presentation of the PLS modeling with case examples – also in the mineral processing field - can be found in MacGregor and Kourti (1995), Dayal and MacGregor (1997a and 1997b), Wold et al. (2001), Hyötyniemi (2001) and Duchesne (2010).

Recursive partial least squares regression was first introduced by Helland *et al.* (1992). The adaptation is based on the update of the PLS covariance matrices when a new observation ($\boldsymbol{x}_t$and $\boldsymbol{y}_t$) is available. The old data are exponentially discounted with the forgetting factor λ_t by updating the

covariance matrices $(\boldsymbol{X}^T\boldsymbol{X})_t$ and $(\boldsymbol{X}^T\boldsymbol{Y})_t$ as follows (Dayal and MacGregor, 1997b):

$$(\boldsymbol{X}^T\boldsymbol{X})_t = \lambda_t(\boldsymbol{X}^T\boldsymbol{X})_{t-1} + \boldsymbol{x}_t^T\boldsymbol{x}_t \qquad (52)$$

$$(\boldsymbol{X}^T\boldsymbol{Y})_t = \lambda_t(\boldsymbol{X}^T\boldsymbol{Y})_{t-1} + \boldsymbol{x}_t^T\boldsymbol{y}_t \qquad (53)$$

Additionally, the forgetting factor can be adjusted continuously, to only discount the old data when the process is persistently excited, thus containing some new information. The variable forgetting factor can be calculated, as shown by Fortescue *et al.* (1981), with

$$\lambda_t = 1 - \frac{\left[1 - x_t(X^TX)_t x_t^T\right]e_t^2}{\sigma_o^2 N_o}, \qquad \lambda_t = \lambda_{\min} \quad if \;\; \lambda_t < \lambda_{\min} \qquad (54)$$

where σ_o^2 is the expected measurement noise variance of the output variable, N_o is the nominal asymptotic memory length (determining the adaptation speed) and e_t is the error between the PLS estimate and the measurement.

3.2 Kalman Filtering Based Process Monitoring

A Kalman filtering method can be applied to reduce the measurement noise and, on the other hand, at the same time to estimate unmeasured process states, when a process model is available. The method was first introduced by Kalman (1960); the algorithm utilizes a discrete state-space system presentation. The computation can be conceived of estimating first the *a-priori* process states $\hat{x}_-$ and then the *a-posteriori* process states $\hat{x}$, when the new process inputs u and the output measurements y are available. The Kalman filtering concept with state-space model matrix notations is illustrated in Figure 9.

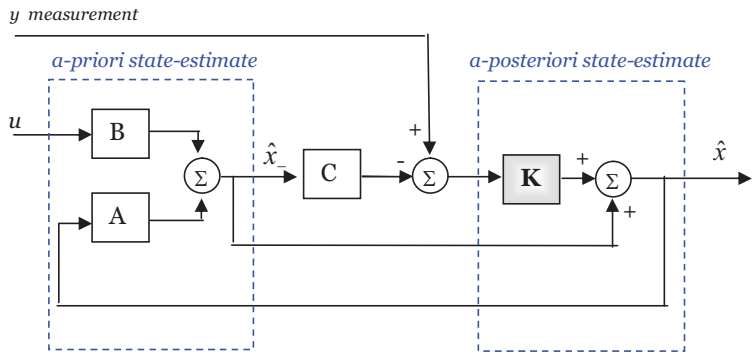

Figure 9. Block presentation of the Kalman filtering with a state-space model. A = state transition matrix, B = input matrix, C = measurement matrix and K = Kalman gain matrix (concept drawn after Welch and Bishop, 2006).

The Kalman filtering consists of two tuning parameters, the covariance of process states Q and the covariance of the process measurements R. In general, both of them are diagonal matrices, finally defining the weighting of the measured and modeled states in the filter output. Kalman filtering is based on minimization of the error covariance of the a-posteriori state estimates. As a result of that minimization, the Kalman gain matrix K is obtained. In case of non-linear process models, an extended Kalman filter, making use of model linearization, can be applied. A more comprehensive introduction on the topic and issues related on practical implementation algorithms of the Kalman filters can be found, for example, in Sorenson (1985), Love (2007) and Grewal and Andrews (2008).

3.3 Model Predictive- and Fuzzy Control of Processes

Model Predictive Control

In model predictive control (MPC) a dynamic process model is utilized to predict the future process responses. These responses are further used in order to optimize the process in terms of a certain cost function. Based on the optimization, the control actions applied into the manipulated variables are determined. The first industrial applications using the early versions of the model predictive control scheme were presented in the late seventies. Nowadays, MPC is widely used especially in the chemical and petrochemical industries. Payback times for the MPC installations are usually reported to be 3-12 months (Perry and Green, 2008). Currently, several variants of the MPC algorisms exist; a good review of them and vendors of the industrial packages can be found in Qin and Badgwell (2003). In addition, a summary of some current MPC and advanced control packages, especially for mineral processing plants, is reviewed in Cipriano

(2010). In general the MPC algorithm minimizes a quadratic objective function J at each time step t

$$J(t) = \sum_{i=1}^{ne} \gamma_y \left[y_r(t+i) - \hat{y}(t+i) \right]^2 + \sum_{j=1}^{nu} \gamma_u \Delta u(t+j-1)^2 . \quad (55)$$

The cost function (55) incorporates the following terms: y_r is the output reference (set point), $\hat{y}$ is the predicted output, Δu is the control increment, *ne* is the prediction horizon length, *nu* is the control horizon length, k is the current discrete time step, the γ_y factors are the output weightings for the control error, and the γ_u factors are the input weightings for the control increments. The optimization is repeated at each time step in a *receding horizon* manner, where only the first computed process input change Δu is realized at a time.

A brief introduction of MPC for the process industries is available, for instance, in Rawlings (2000), Bequette (2003) and Qin and Badgwell (2003), all of them handling briefly also the nonlinear MCP schemes. Nonlinear model predictive control is introduced more extensively, for example, in Findeisen and Allgöwer (2002), who outline theoretical aspects; Bequette (2007) describes implementation practices and underlies some of the common "pitfalls"; and Diehl et. al (2008) provide an overview the computational issues.

Qin and Badgwell (2003) have anticipated that in the upcoming MPC applications the practical control engineering issues, related to commissioning and tuning for instance, have a greater importance instead of the algorithm development issues. They have foreseen that the process models involved in the MPC are to be constructed with a graphical representation of the plant, comprising continuous-time fundamental models.

Fuzzy Control

Fuzzy logic is used to model the decision making of human operators, having expert knowledge of the process. A fuzzy logic controller is set up by defining certain ranges for variables, having non-crisp ranges with linguistic descriptions. An example of such a variable fuzzification is shown in Figure 10, where a flotation column grade, recovery and aeration rates are classified to triangular shape fuzzy sets. The fuzzified inputs and outputs are linked by setting up an if-then rule-base. Finally the controller output is computed by a defuzzification procedure, where the degrees of the membership of each input in the output sets are determined. A common

method is to calculate the centre of gravity of the sets, as shown also in the example of Figure 10, where the resulting column air setpoint is about 53 %. The computed output of a fuzzy controller is fully deterministic, contrary to the popular belief.

The history of fuzzy logic starts in the mid-nineteen sixties in the work of Lofti Zadeh. An introduction to the topic can be found, for example, in Lin and Lee (1996) and Love (2007); case examples of fuzzy control of mineral flotation columns are presented in Bergh et. al (1998), Bergh et. al (1999), Carvalho and Durão, (2002) and Núñez et. al (2010).

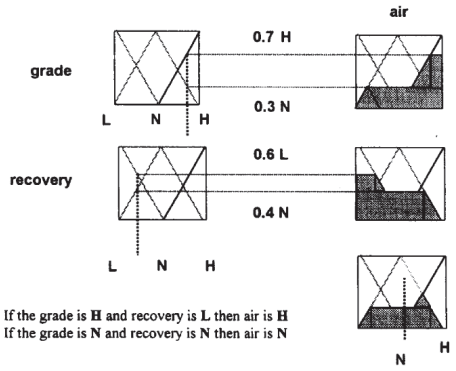

Figure 10. An example of fuzzification, inference and defuzzification; grade and recovery are fuzzified into the sets: L=low, N=normal and H=high, inference rules are applied, and after defuzzification the air setpoint for the flotation column is obtained (Bergh et al., 1998).

A drawback in setting up a large fuzzy control system is the tedious tuning work. However, adjustment of the parameters is still feasible if the number of rules is kept sufficiently small (Carvalho and Durão, 2002). In addition to that, another important parameter affecting also the control rules is the selection of the control period (Bergh, et al., 1998). The control cycle should be chosen based both on the process dynamics and the constraints set by the process measurements. Recently in the case of the Minera Los Pelambres (Chile) flotation column fuzzy control, Núñez et. al (2010) addresses the controller tuning still as a research area in order to improve the controller response time.

4 Description of the Application Process Plants

4.1 Kemi Chromite Concentrator

Geology and Production

The Kemi layered intrusion, containing the chromite deposit, is about 15 km long and 0.2 to 2 km wide. The chromite deposit is the largest of all mineral deposits in Finland, having 162 Mt estimated resources at 26 % Cr_2O_3. In addition to chromite, the ore contains serpentine, amphiboles, talc and carbonates as the primary gangue minerals. The natural size of the chromite grains varies greatly, and is characterized by microcracking and brokenness; in minerals procesing this reduces the size of purely ground chromite (Huhtelin, 2007). The chromitite in Kemi was first found in 1959 during excavation of a fresh-water channel. The open pit mining started in 1966, and the underground production in 2003, being the only mining method since 2006. The concentrator products are upgraded lumpy ore and metallurgical grade concentrate. Table 1 summarizes the production of the Outokumpu Chrome Oy Kemi Mine. (Huhtelin, 2007; Geological Survey of Finland, 2010b)

Table 1. Production of the Outokumpu Chrome Oy Kemi Mine.

Annual ore feed: 1.2 Mt Cr_2O_3: 26 %			
Product	**Annual production**	**Grade**	**Grain size**
Upgraded lumpy ore	200 000 t	35 % Cr_2O_3	12-100 mm
Fine concentrate	350 000 t	45 % Cr_2O_3	0.2 mm

Minerals Processing Plant

The Kemi concentrator consists of crushing, dense medium separation and concentration sections. After separation of the lumpy ore by a sink-float circuit in the dense medium separation, the crushed ore is fed to the concentration section. First, the crushed ore is processed in a rod mill - ball mill grinding mills in a closed circuit with an 800 μm screen. The concentrating stage consists of Reichert cones and spiral separators. Fine slime, separated with hydrocyclones, is further processed in a high-gradient magnetic separation (HGMS) circuit. A process flowsheet of the Kemi concentrating plant is shown in Figure 11.

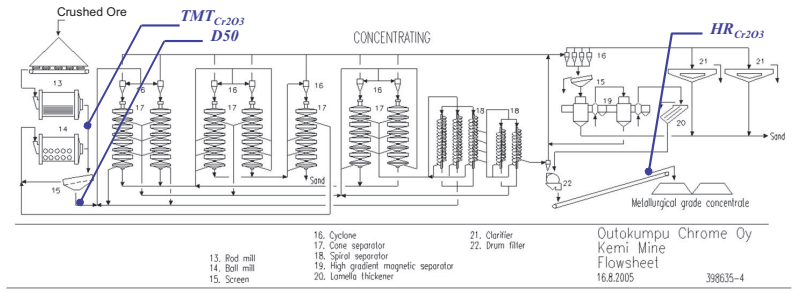

Figure 11. Flowsheet of the Kemi concentrating plant; notations of selected process sampling points: TMT_{Cr2O3} = rod mill discharge assay, HR_{Cr2O3} = fine concentrate assay and *D50* = particle size analysis. (original CAD image: courtecy of Outokumpu Chrome Oy)

The Kemi Mine is integrated to the ferrochrome smelter of Outokumpu Tornio Works, located 20 km from the mine. The high chromite grade of the concentrate is advantageous for ferrochrome production. Therefore the main operating goal at the Kemi Mine is to maximize the chromite content of the concentrate, used subsequently in the ferrochrome smelter, while keeping the concentrate production rate at a predefined value.

4.2 Siilinjärvi Phosphate Concentrator

Geology and Production

The main minerals in the Siilinjärvi ore deposit are 10 % of apatite, 20 % of carbonates (calcite and dolomite) and 65 % of phlogopite mica. The first findings of the ore were made during construction of the Siilinjärvi-Sysmäjärvi railroad connection in 1950. Later on production at the Siilinjärvi open pit mine started in 1980; now the open pit is around 2.8 km long and 200-700m wide. Currently, Siilinjärvi is the largest industrial mineral mine in Finland and also the only phosphate mine in Western Europe. It processes annually around 10 Mt of ore; more than 200 Mt of ore resources are still estimated to be available. Table 2 summarizes the production of the Yara Siilinjärvi Mine. (Geological Survey of Finland, 2010a; Yara, 2010; Kemira, 2005)

Table 2. Production of the Yara Siilinjärvi Mine.

Annual ore feed: 10 Mt P_2O_5: 4 %. Apatite 10 %, Carbonates (calcite + dolomite) 20 %, Phlogopite mica 65 %		
Product	**Annual production**	**Grade**
Apatite concentrate	800 000 t	36.5 % P_2O_5
Calcite concentrate	100 000 t	-
Mica	10 000 t	-

Minerals Processing Plant

At the Siilinjärvi concentrator the ore is first crushed in a three-stage crushing section, followed by homogenization with a stacker-reclaimer system. The grinding section consists of two parallel rod mill – ball mill circuits. Next, the apatite is separated in two parallel flotation circuits and purified with a high gradient magnetic separator. Finally, dewatering is carried out by thickening and filtration. The concentrator flowsheet is shown in Figure 12.

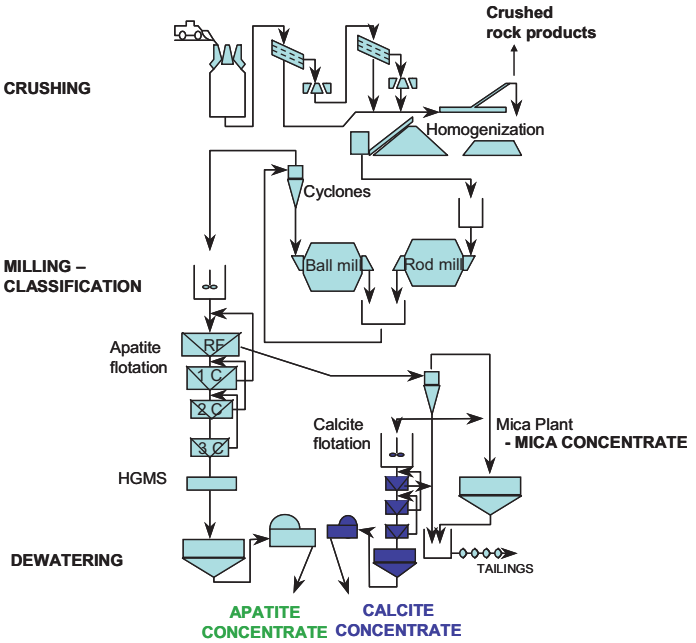

Figure 12. Flowsheet of the Yara Siilinjärvi concentrator. (courtesy of Yara Suomi Oy)

The capacity of the concentrator depends greatly on the ore type. Especially the carbonates/mica ratio has a major impact on grindability; the average is around 0.3, but can vary between 0.15 and 0.7. The produced apatite concentrate is used totally in the phosphoric acid and fertilizer plants, integrated with the mine.

4.3 Pyhäsalmi Copper-Zinc-Pyrite Concentrator

Geology and Production

The Pyhäsalmi deposit is one of the largest metallic mineral deposits in Finland. It is of VMS (volcanogenic massive sulphide) type of ore. The ore is mainly composed of sphalerite ($Zn_{0.95}Fe_{0.05}S$), chalcopyrite ($CuFeS_2$) and pyrite (FeS_2). The ore was found in 1958 when a local farmer was blasting rock in order to establish a water well. Interesting looking samples led soon to test drilling by Outokumpu Oy. Construction of the mine started next

year, and the open pit mine started operating in 1962. Thereafter, underground mining was started in 1967. A new significant deep ore deposit was found in 1996 and the current expectation is to have the ore resources until 2018. Annually the concentrator processes 1.4 Mt of ore. Table 3 summarizes the production of the Inmet Mining Corporation Pyhäsalmi Mine. (Saltikoff et al., 2006; Mäki, 2008; Inmet Mining Co., 2010; Webmineral, 2010)

Table 3. Production of the Pyhäsalmi Mine Oy (Inmet Mining Co., 2010).

Annual ore feed: 1.4 Mt Cu: 1.1 %, Zn: 2.2 %, S: 41 %		
Product	**Annual production**	**Grade**
Copper concentrate	50 000 t	29.0 % Cu
Zinc concentrate	70 000 t	54.0 % Zn
Pyrite concentrate	600 000 t	51.0 % S

Minerals Processing Plant

At the Pyhäsalmi plant, the ore is crushed in the underground mine. In the concentrator the crushed ore is first screened into lump, pebble and crushed fine ore. In the grinding section, the primary grinding is carried out in a semiautogenous (SAG) mill. Secondary and tertiary grinding stages are in a closed circuit with hydrocyclones. The hydrocyclone overflow is fed into sequential flotation circuits, where the copper, zinc and pyrite concentrates are separated selectively. Finally, the concentrate slurries are thickened and filtered in the dewatering section. A flowsheet of the concentrator is shown in Figure 13.

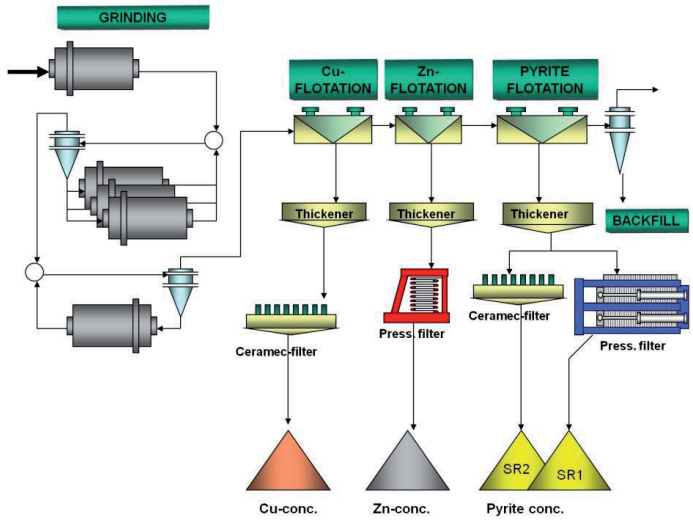

Figure 13. Flowsheet of the Pyhäsalmi concentrator. (courtecy of Pyhäsalmi Mine Oy)

5 Case Applications – Experimental

5.1 Introduction to Experiments

The process modeling, monitoring and control methods applied in this thesis were pilot tested based on the process data of three Finnish mineral concentrator plants. The plants are located in Kemi, Siilinjärvi and Pyhäsalmi; brief descriptions of the processes are given in Chapter 4. All the case applications cover modeling of the process to some extent. Therefore, prior to the studies, process experiments and data gathering periods were undertaken. In the following, the plant experiments and the exploited data periods are described.

5.1.1 Process Experiments at the Kemi Concentrator

Grinding circuit

The grinding - gravity concentration process monitoring method described in this thesis was constructed based on a data set of January-February 2006. During the data collection, the grinding circuit control variables – the ore feed rate and the rod mill rotation speed – were varied stepwise to enhance the excitation of the data. In addition, slurry samples and crushed ore samples from the grinding circuit were collected in order to determine variations of the ore type and the amount of the circulating load. Figure 14 presents a flowsheet of the grinding circuit with the location of the automatic on-line particle size measurement sampling point. Selected variables of the collected data set, described in [P1], are shown in [P3].

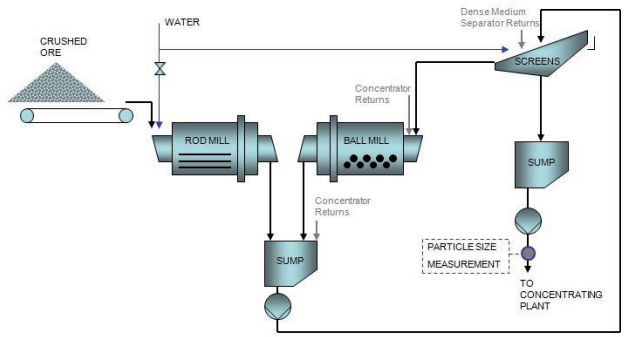

Figure 14. Flowsheet of the Kemi concentrator grinding circuit.

5.1.2 Process Experiments at the Siilinjärvi Concentrator

Grinding Circuit

To find out the dynamic responses of the grinding circuit to the changes in the control variables, a series of step response experiments were carried out while running several individual ore feed heaps. The experiments were carried out during February - March 2008, covering six days with slightly different ores. The carbonate/mica ratio varied between 0.35 - 0.49, which represents fairly typical Siilinjärvi ore characteristics.

The experiments were conducted with the smaller capacity grinding circuit (J1), while the second circuit (J2) was running normally. Both primary and secondary mill slurry densities were controlled by mill water addition. The circuit product slurry density – which is a calculated quantity – was controlled by manipulating the sump water addition valve. The circuit product particle size distribution was monitored with an on-line *Outotec PSI 500™* particle size analyzer. In addition, to inspect the analyzer operation, laboratory slurry samples from the analyzer calibration sampler were collected for each stabilized operation region. Figure 15 presents the grinding circuit flowsheet with major measurements and the points (A, B and C) where the step changes were applied. The stepwise inputs were:

- A) Ore feed rate: from an average of 500 t/h ± 50 to 100 t/h.
- B) Circuit product slurry density / sump water addition: from an average density of 1360 kg/dm3 ± 30 to 40 kg/dm3.
- C) Number of cyclones in use: variations between 6 and 8.

An example data set of the applied step changes and the measured grinding circuit discharge particle size responses is presented in [P7].

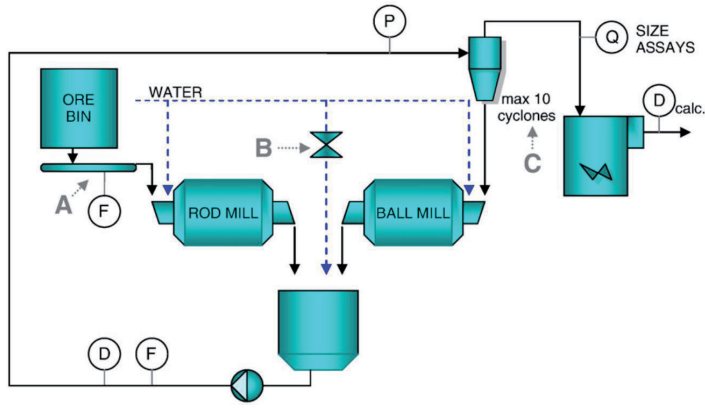

Figure 15. Siilinjärvi grinding circuit and the applied step responses: A) ore feed rate, B) sump water addition C) number of hydrocyclones in action.

Apatite Concentrate Thickener

The applied thickener monitoring scheme (see Section 5.2.1) was tested by conducting flow rate manipulation experiments (26 May 2009). The thickener volumetric underflow rate set point was varied between 110 – 90 – 110 m^3/h. Also the filtration backflow feed rate was affected by taking one more pressure filter into action, in addition to the drum filter; this reduced the flow back to the thickener. Furthermore, the fresh feed flow from the high gradient magnetic separator (HGMS) had a variation due to the operation of the preceding process stages. The applied input manipulations and the thickener response are presented in [P6].

5.1.3 Process Experiments at the Pyhäsalmi Concentrator

Floatex density separator

Aim of the pilot test at the Pyhäsalmi Mine was to study the feasibility of separating the pyrite concentrate into fine and coarse fractions with certain specifications by using a hindered settling classifier. The plant personnel carried out the experiments in March 2010 with a pilot Floatex unit of 0.89 m hydrostatic height and 0.46 m side length. The equipment included a pressure sensor connected with a bed pressure controller manipulating the underflow discharge valve. The teeter water flow rate was stabilized as well.

The feed-, overflow- and underflow compositions and flowrates were measured by collecting samples manually. The feed consists of pyrite slurry having an average density of 1910 kg/m^3 and a flow rate around 2.5 t/h. The feed size distribution was typically 63.5 % of -74 µm fraction, while the 80 % passing size was 104 µm. The solids density of the pyrite (FeS_2) concentrate was 5000 kg/m^3. The sieve analysis covered screen sizes: 20, 37, 74, 105 and 149 µm. The pilot Floatex was operated in several operating points by varying the bed pressure between 11...13 kPa and teeter water flows from 25 l/min up to 60 l/min; the obtained data are presented in [P8]. A schematic diagram of the test apparatus is shown in Figure 4.

5.2 Modeling and Monitoring of the Selected Unit Processes

5.2.1 Concentrate Thickener

At the Siilinjärvi concentrator the apatite concentrate slurry is dewatered with a 20 m diameter thickener followed by a drum and pressure filters (see the flowsheet in Figure 12). Occasionally, the thickening operation suffers disturbances, which may originate from the ore type variations, slurry particle size variations, varying slurry flow rates or uneven sedimentation flow pattern. The disturbances cause changes in the thickener solids mass throughput and water overflow rates. Also, water short-circuiting from the

clarification zone to the underflow can occur. Finally, the operational problems can lead to a pressure drop in the underflow cone, a rapid increase in the raking arm moment, underflow slurry pump cavitations and too low and/or uneven underflow slurry density. The disturbance periods can last from less than an hour up to several days.

Therefore, the aim of the process development was to be able to monitor the thickener operation in more details to detect the upcoming disturbances earlier. In that way it may be possible to react to them and avoid or reduce the unwanted underflow fluctuations. The applied model is based on a total solids mass balance and water balance. Due to the presumed inaccuracies in the underflow mass flow measurement, the flow rate was also calculated from the volumetric flow balances, assuming the overflow to be clear water. The model applies Equations (37) to (45), the notations are shown also in the schematic diagram of the thickener in Figure 16a.

In addition to the solids mass, the water flow rates and the solids flow rates, the average density of the thickener content and thus the underflow pressure were also calculated. The model was utilized in Kalman filtering, where the underflow mass flow rate and the pressure of the underflow cone were the measured output variables. Operation of the soft-sensor set up was tested with the flow rate manipulation experiments (26 of May 2009) described in Section 5.1.2 and in [P6]. The monitoring application was thereafter implemented into the plant automation system. Figure 16b shows the application user interface providing both the measured and estimated thickener state information for the plant operators.

The system has been discovered to be useful in the daily plant operation; especially the estimated solids mass accumulation and the deviation in the estimated and measured cone pressure provides valuable information of possible progressing process disturbances (Aaltonen, 2010).

a) b)

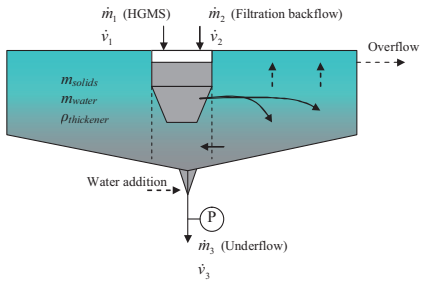

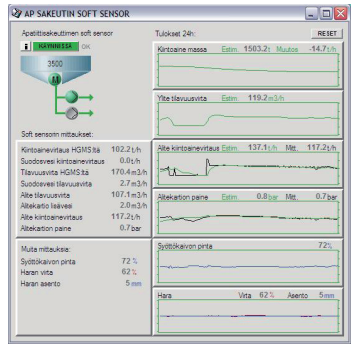

Figure 16. Siilinjärvi thickener monitoring case: a) schematic figure showing the thickener streams and notations, b) operator interface window of the implemented monitoring tool (Courtesy of Yara Suomi Oy).

An example of a typical apatite concentrate thickening disturbance at Siilinjärvi (data period: May 2009), where the mass accumulation occurs, is shown in Figure 17. The figure shows an eighteen hours time period where the mass accumulation (a Kalman filter estimated value) has started around time 2 h. The accumulation has accelerated even more due to an increased feed flow from the high gradient magnetic separator (HGMS) after time 7 h. It is also possible that the mass has accumulated to the edges of the thickener, causing water short-circuiting. This may have caused the drop of the slurry underflow density and the increased rake torque, seen after the 9h time point.

To normalize the operation, the rake arms have been raised, and also a secondary underflow pump has been started. This can also be seen from the increased filtration backflow and overflow water rates. The disturbance shown in Figure 17 has obviously included also slurry pump cavitation, as seen from the volumetric underflow rate drop around 11.5 h. Finally, the secondary pumping drastically unloads the accumulated mass. The secondary pumping has been stopped after the primary underflow rate has reached the normal operation target.

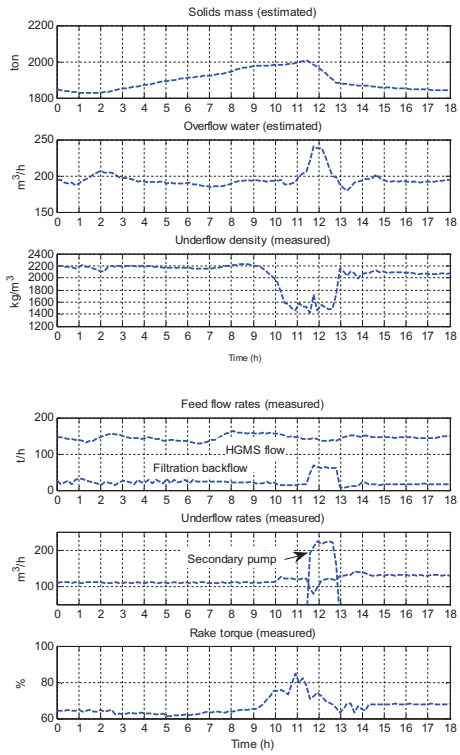

Figure 17. Siilinjärvi thickener monitoring case: example of a propagating process disturbance due to excessive solids mass accumulation, leading to relatively sudden drop of the underflow density.

Novelty of the Method

The inferred information of the thickener solids mass is valuable for maintaining optimal operating conditions and preventing upcoming disturbances. Neither the slurry level measurement, the bottom cone pressure measurement nor the underflow slurry density measurement alone give that information themselves. By utilizing the existing process measurements a relatively simple and straightforwardly implementable method for estimation of the key physical quantities of a mineral slurry thickener can be obtained. The computation is based on the well-known and proven Kalman filtering technique. The monitoring concept of the industrial mineral concentrate thickener operation, applied in the Siilinjärvi case, have not been previously reported as such in literature.

5.2.2 Floatex Density Separator

Operation of the Floatex fluidized bed separators was studied by applying the model equations (2) – (21). The case examples cover a model calibrated with a pilot scale equipment data, and a model parameterized to describe the operation of the existing plant scale equipment.

Pyhäsalmi Pilot Scale Pyrite Concentrate Separator

The model of the Pyhäsalmi pilot pyrite separator was calibrated based on the experimental data described in Section 5.1.3 and in [P8]. First, separation efficiency curves, describing the partition of the feed reporting into the underflow as a function of the particle size, were determined for each experiment data set. Subsequently, the effect of the bypass of fines was compensated for by applying (21) conversely, to obtain corrected efficiency curves from the data. In addition, the corrected cut-sizes were determined. Next, the efficiency curve of form (18) was fitted to the data, the stochastic movement of the particle slip velocity $\sigma_{v,slip}$ (m/s) being a free parameter. Further, the parameter $\sigma_{v,slip}$ was correlated with the operating point of the Floatex, namely teeter water interstitial velocity. Another separation efficiency model parameter, the bypass fraction r, used in (21) was also determined from the experimental data. The bypass of fines has a functional correlation with the total underflow fraction of the solids feed. The model parameter correlations, defining the separation efficiency characteristics of the Pyhäsalmi pilot case, are shown in Figure 18.

a) b)

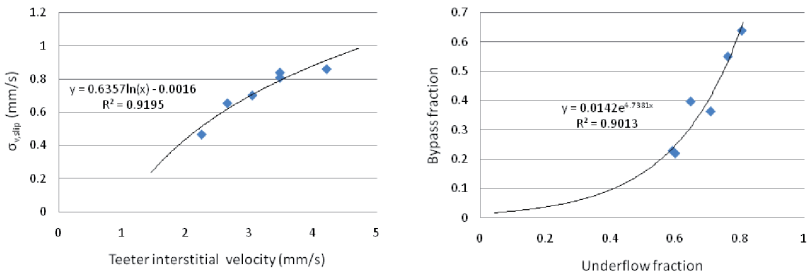

Figure 18. Pyhäsalmi pilot Floatex case: experimental correlation of a) particle slip velocity standard deviation as a function of teeter interstitial velocity and b) underflow stream bypass fraction as a function of solids fraction reporting to underflow, for pyrite mineral particles.

The simulations covered operating points ranging between 10…13 kPa bed pressures and 20…60 l/min teeter water flowrates. The feed particle size distribution, modeled using the *Rosin-Rammler* cumulative distribution curve, was set to yield 32 % of a -37 µm fraction, 63.5 % of a -74 µm fraction, while the 50 % passing size was 56.6 µm. The size compositions and mass flow rates of the underflow and overflow streams were computed. Calculation of the stream compositions was carried out in an iterative manner, since the underflow fraction depends on the empirical correlation of the bypass fraction r (Figure 18b). In addition, the underflow slurry density was determined based on a correlation derived from the experimental data.

Results of the simulations are presented in Figure 19. Figure 19a describes the separation efficiency of the corrected efficiency curve in terms of *Ecart probable* E_p, covering the manipulated bed pressure and teeter water operating points. The Ecart probable indicates the separation curve steepness by using particle sizes of 75 % and 25 % partitions to underflow: $E_p = \frac{d_{75}-d_{25}}{2}$. Thus Figure 19a presents equation (18) in each cut-size and operating conditions of the simulation. Subsequently, when the bypass effect (21) is taken into account, the separation efficiency of the fines decreases significantly especially under low teeter water and low bed pressure conditions. Here, the main interest was in the prediction of the separation performance of the fine -37 µm fraction. Hence, Figure 19b presents the recovery of the feed -37 µm material to the overflow.

In addition, the cut-size surface of the separation (referring to the *corrected cut size*) is presented in Figure 19c. Correspondingly, Figure 19d shows the percentage of the -37 µm fraction of the overflow stream. It can be noted, that the parameterized separation efficiency characteristics bring also nonlinearity into the obtained size fraction response surface. A high portion of fines in the overflow stream causes, on the other hand, a high fraction of the feed reporting to the underflow, shown in Figure 19e. Especially, low teeter water flow, causing insufficient fluidization, results in high solids recovery to the underflow even with high bed pressures. Vice versa, high teeter water flow rates cause high underflow slurry densities already with moderate bed pressures as seen from Figure 19f.

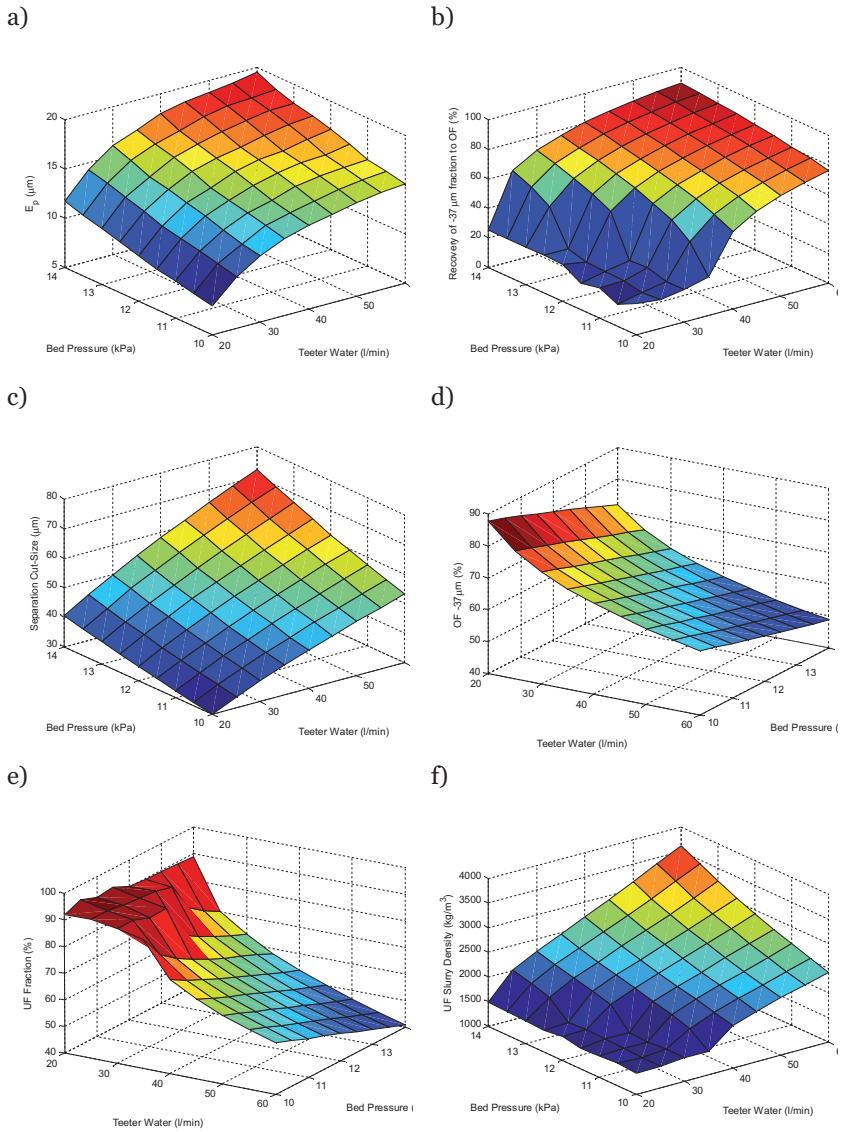

Figure 19. Simulated Floatex performance surfaces of the Pyhäsalmi pilot case in terms of teeter water flow rate (l/min) and bed pressure (kPa); a) Ecart probable separation efficiency, b) recovery of under 37 µm fraction from feed to overflow, c) Cut-size of the separation (µm), d) overflow fraction (%) of under 37 µm, e) fraction of feed solids to underflow stream (%) and f) slurry density of the underflow stream (kg/m3).

Siilinjärvi Industrial Scale Ground Ore Separator

In addition to the above presented simulation of the Pyhäsalmi pilot scale separation of one mineral species, a feasibility study for simulation of a multicomponent system with non-spherical particles was carried out. In that set up it was also possible to calculate the mineralogical composition of the underflow and overflow streams of the hindered settling classifier. Such a computation was tested using specifications corresponding to the

Siilinjärvi Floatex separators. The separators are currently installed in a closed circuit with the ball mill grinding mills, since the concentrator flowsheet was modified in 2009 from that presented in Figure 12. For simplicity, the model was parameterized using constant slip velocity standard deviation. The feed composition was parameterized based on the earlier laboratory sample results available. Passing sizes of the feed size distribution were set to P50 = 550 µm, P80 = 1200 µm, when the -74 µm proportion was 8 %. The feed consists of apatite (AP) 10 %, carbonate (KRB) 20 % and phlogopite (FLG) 70 %. The feed composition analysis by size fractions is shown in Figure 20a. In addition, the specific gravities and particle shape factors of each mineral were also defined; the mineral parameter setup was:

- Specific gravities: AP 3200 kg/m^3, KRB 2750 kg/m^3, FLG 2850 kg/m^3.
- Particle shape factors: AP 1, KRB 1, FLG 0.6.
- Separation efficiency parameter, standard deviations of slip velocities: AP 3 mm/s, KRB 3 mm/s, FLG 4.5 mm/s.

In addition to the total size distribution of the output streams, the size distributions of each mineral could be computed. Figure 20b shows a result of the mineral specific overflow size distributions when the above parameterization of the feed composition (Figure 20a) were used. For operation of the grinding circuit, estimation of the products mineral specific sizes is advantageous. The estimation method based on the Floatex model equations has a great potential to optimize the grinding operation, keeping the distribution of the valuable mineral optimal for the flotation.

a) b)

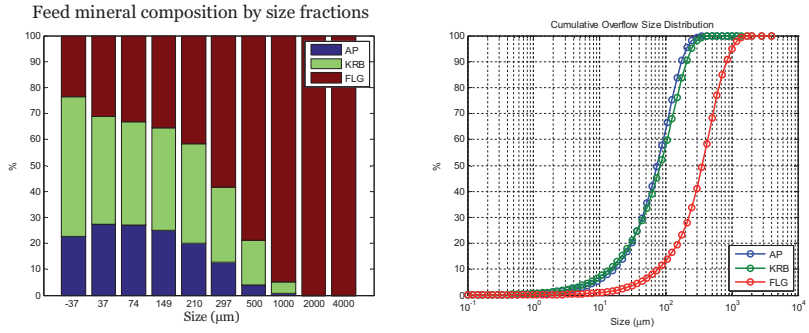

Figure 20. Simulation of the Siilinjärvi Floatex operation; a) specified feed mineral composition into the separator, b) simulated Floatex overflow stream cumulative particle size distributions of each mineral (AP = apatite, KRB = carbonate, FLG = phlogopite).

Novelty of the Method

In literature, most of the studies of the hindered settling separation in the Floatex density separators concern separation of coal slurries. Here, two

mineral concentrator application cases with the existing model structures were set up. The novelty of the modeling approach comes in the application of both slip velocity based particle movement calculation and the stochastic separation efficiency formula to determine whether a particle is reported to the under- or overflow. In addition, the computation of the separate size distributions of three minerals into the under- and overflow was demonstrated in the Siilinjärvi case example. In future, industrial scale modeling of the separation of each mineral needs still to be validated with a laboratory sampling campaign.

5.3 Plant-wide Monitoring Case Study

This thesis includes one case study, where a plant-wide process monitoring was demonstrated. The case process is at the Kemi concentrator, consisting of the grinding and gravity separation circuits. The collected time series consists of 153 samples of ten-minute average data. The output variable is the concentrate grade HR_{Cr2O3} (expressed in $\%Cr_2O_3$), measured by an on-belt XRF analyzer after the drum filter (see Figure 11). The selected input variables were the feed slurry chromite on-line assay ($\%Cr_2O_3$, TMT_{Cr2O3} in Figure 11) and the on-line analysis of the 50 % passing size of the particles (µm) (*D50* in Figure 11), measured from the grinding circuit. In addition, to describe the ore in terms of grindability, the Bond operating work index (kWh/t) (*WIo*) was calculated by applying (Napier-Munn *et al.*, 2005)

$$WIo = \frac{W}{10\left(\frac{1}{\sqrt{P_{80}}} - \frac{1}{\sqrt{F_{80}}}\right)} \qquad (56)$$

where W (kWh/t) is the work input of the grinding mills and P_{80} and F_{80} (µm) are the 80 % passing sizes of the grinding circuit's product slurry and the ore feed respectively.

The process was modeled using a recursive partial least squares method Eq. (52) – (54). The model structure for the Kemi plant, incorporating the grinding and gravity separation stages, is illustrated in Figure 21. The model dynamics was obtained by including a one step backward output estimate as one input of the system. For adaptation of the model parameters, thus changing the λ_t in Eq. (54), the effective memory length N was set to 10 (standing for a 1.67 hours time slot), and the expected measurement noise of the output variable σ_0^2 was set to 0.04. The minimum value limit for the forgetting factor was set to 0.85. The first 15

data samples were used for calculation of the initial values of the covariance matrices.

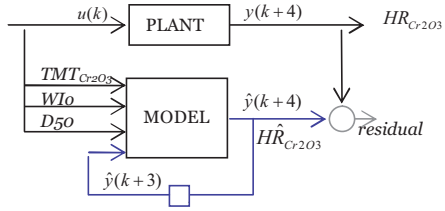

Figure 21. A scheme of the model structure for the Kemi grinding-gravity separation plant.

Evolution of the model regression coefficients for the data set is shown in Figure 22a, while Figure 22b shows the evolution of the forgetting factor, affecting the speed of the coefficient adaptation. The regression coefficients change abnormally between samples 60-80; this is probably due to a failure in the chromite assay slurry sampler, causing the sudden change in the measurement. That can be deduced also from the original data in [P3].

a) b)

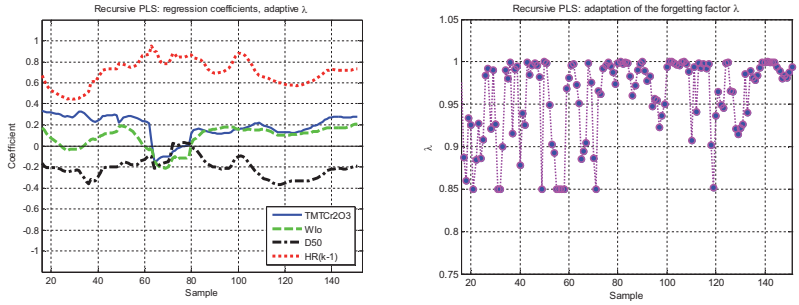

Figure 22. Adaptation of the model parameters in the plant-wide monitoring model for the Kemi gravity concentrator; a) regression coefficients of the PLS model b) forgetting factor, defining the adaptation speed; the sample interval is 10 minutes, thus the length of the data set is approximately 26 hours.

Next, the original time varying model parameters, shown in Figure 22a, were used for the calculation of the impacts of the changes in the input variables. Table 4 summarizes the effects of the changes in the model input variables on the predicted PLS model output, in terms of original unscaled Cr_2O_3 (%) concentrate grades. The listed numbers indicate the change of the model output resulting from a 10 % increase of each input from its mean value, respectively. It can be seen that the feed chromite content (TMT_{Cr2O3}) and the particle size ($D50$) cause the largest responses on the estimate of the concentrate grade, but in opposite directions. However, the magnitude of the impact of the inputs, and even a sign of the impact, can change drastically during the process operation, as seen from Figure 22a. Thus, an adaptive, model-based on-line monitoring system can give valuable information in advance, regarding the favorable control actions in the

beginning of the process chain. The operation parameters in the gravity concentration section were assumed to be unchanged during the time span. The adaptive model scheme can be useful, for example, in deciding the optimal grinding fineness in changing ore type conditions. Similarly, in the on-line use of the adaptive model, the current input variable coefficients indicate the impact of each input on the concentrate grade, since the gravity separation control variables are kept unchanged.

Table 4. Simulated net changes in the chromite concentrate grade for the whole 23 hours time period, when 10 % increase of each input variable were applied respectively; pre-calculated varying model parameters were applied.

Input variable	10 % of the variable's mean	$\Delta\hat{H}R_{Cr2O3}$ (%) when the input change is 10 % of the mean
TMT_{Cr2O3}	2.6	0.26
Wlo	1.0	0.08
D50	6.7	-0.19

Novelty of the Method

A data-based method for a plant-wide monitoring was applied based on the well-known and computationally robust linear recursive partial least squares model with a dynamic model structure. The monitoring scheme was demonstrated with data from a grinding-gravity separation process chain. This type of monitoring scheme has not been reported earlier. The main advantage is to gain prior knowledge of the favorable directions of the control actions in the grinding circuit, based on the adaptation of the model parameters. This has especially potential in determination of the optimal grinding fineness, in the cases when the ore type is changing and the grain size of the valuable mineral is unknown. An early response in the grinding stage can reduce the fluctuation of the concentrate grade and the losses in recovery.

5.4 Control Studies of the Mineral Processing Cases

This chapter describes the control studies of grinding and flotation circuits of simulated and real mineral processing plants. First, preliminary surveys exposing the characteristics, limitations and applicability of the selected control systems, when applied into mineral processing, were carried out. Then a novel model-based control system for stabilizing both the circuit outlet slurry particle size and the circulating load at the Siilinjärvi grinding process was formulated. Advantages of the presented system were pointed out by simulations.

5.4.1 Preliminary Surveys of Advanced Control Feasibilities and Benefits

The preliminary control studies were carried out to gather information from simulated and experimental implementations of the common rule-based and model-based control methods in mineral processing applications. The cases cover studies of the impact of a rule-based expert system and a model predictive control on performance of *flotation* processes with different configuration setups. Also, a practical experiment of the control of a *grinding* circuit outlet slurry particle size by manipulating the mill rotation speed was carried out. Finally, a control simulation study with a simplified *grinding – flotation* model was also performed.

I) Effect of an Expert Control System and Model-Based Control on Flotation Performance

The flotation control with base-layer stabilization and high-level advanced optimization was first studied with a flotation process simulator. The flotation circuit simulations were set up with HSC-Sim® dynamic flotation flow sheet simulator, in connection with an expert control system. The applied simulator partly incorporates the flotation kinetics, in manners described in Section 2.3. The simulated copper flotation circuit was set up with closed loop rougher-, scavenger and cleaner stages, shown in [P5].

The base-layer control system, implemented in the simulator environment, includes cell level feedback controllers combined with feed forward controllers, compensating for the fluctuations originating from the feed. The higher level expert controller utilizes the feed-, tailings- and concentrate Cu assays, and the froth speed measurements of each cell, available from the simulator. The control variables were the cell levels and the aeration rates. The rule-based control hierarchy was set up as follows:

- Froth velocity set points were calculated based on Cu assays, the aim was to keep the concentrate and tailings Cu-% within predefined limits.
- The froth velocity in each cell was maintained by manipulating the aeration rates and the cell levels.

The targets for the control system were to keep the concentrate grade above 29 %-Cu and the tailings at less than 0.043 %-Cu. Four different simulation cases were run with a setup interconnecting the simulator and an advanced control platform: simulation without the cell level or aeration setpoint changes, control with a 10 minutes interval, control with a 30 minutes interval, and finally control with a 30 min interval with additional measurement errors of 10 rel.-% and 7 rel.-% for the concentrate and tailings respectively. An eight hours dataset consisting varying feed Cu grades (%) and the feed rates (t/h), obtained from a real process plant, were

the inputs for each of the simulations. The results of the simulations are summarized in Table 5 in terms of the grade, recovery, and the total mass of the recovered copper on a daily basis. Roughly, advanced control increased the recovery by nearly a 1% unit compared to the base case.

Table 5. Results of the simulated flotation control cases.

Simulation Case	Concentrate grade (Cu-%)	Recovery (%)	Total Cu tons/day in concentrate
Base case: manual operation, setpoints unchanged	28.6	91.8	124.5
Expert control: 10 min assay delay	29.2	92.6	125.6
Expert control: 30 min assay delay	29.2	92.6	125.5
Expert control: 30 min assay delay and decreased assay accuracy	29.3	92.4	125.4

In addition, another study assessing the effect of the control interval for both the rule-based and the model predictive control was carried out in [P2]. The applied simulated flotation process is described in Hodouin et al. (2000). The process disturbances originated from variations of the feed grade and the flow rate, the manipulated variables were the air feed rate and the collector flow rate. The control interval was varied based on different assay delay cases. The control performance was evaluated based on the ISE (integral square error) index, when set point changes and input disturbances were applied in the simulations. As expected the longer assay delay (from 6 to 30 min) decreases the control performance. More significant was the finding that a change from the rule-based control to the model predictive control typically decreased the variation in controlled variables more than 50%.

Observations Based on the Study

This study pointed out that a simulation model with detailed flotation kinetics is well suited for control studies examining different setups in similarly repeatable process conditions. The benefits are obvious, when developing control strategies for an existing or a new flotation plant. Besides, the case study demonstrated the advantages of an expert control system for a flotation circuit, based on manipulation of the froth speed, even though the control algorithm was kept relatively straightforward.

II) Benefits and Limitations of the Particle Size Control - Case in Practice

Use of the on-line particle size analysis in the grinding control was studied at the Kemi concentrator. A rule-based particle size – rod mill rotation speed control system was set up and the operation of that in practice was tested in various process conditions, described in [P4]. The on-line particle size control was tested in two periods. In both of them, the rule-based control interval was set to 45 minutes, allowing also the return flows from the Reichert cones to stabilize. The aim was to keep the particle size D50 passing size at the 40 μm set point, measured with an on-line analyzer. At around 250 minutes (Figure 23a) the effect of a change in the ore type (fed from the separate ore bins to the crushed ore heap: from VVPohja2 to Mama1) starts to appear in the response of the particle size. It can be seen that the control actions could not keep the process in the original set point (minimum mill rotation speed is approximately 12 RPM), and the set point was changed at 390 min to 35 μm, being more suitable for that ore type.

The next operating period was run from Mama1 ore bin (Figure 23b). The data set includes a measurement break around 330-420 minutes; subsequently causing one erroneous control action pointed out in Figure 23b. However, during the test period the particle size was successfully kept near the set point. When compared to the manually operated grinding adjustments, the rule-based variable mill rotation speed control decreases the particle size standard deviation on average by more than 20 %.

a)

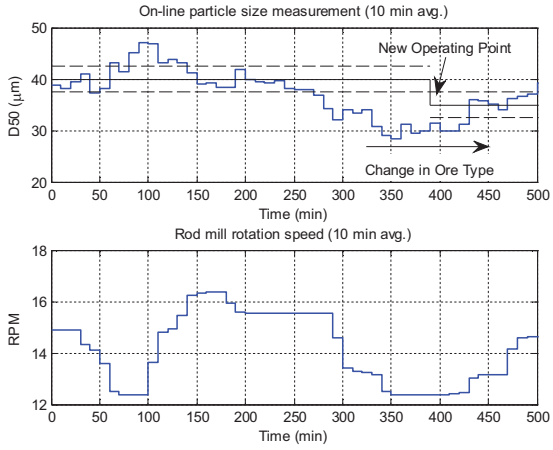

b)

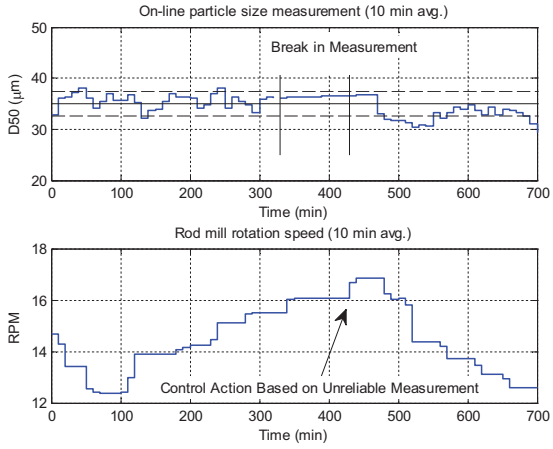

Figure 23. Control of the Kemi grinding circuit product particle size by manipulating the rod mill rotation speed. a) 1st of November 2007 and b) 2nd of November 2007.

Observations Based on the Study

This practical control study addressed the significance of a proper data pre-processing and an on-line analysis validity assessment. Still, the experiments proved that the variation in the ground product particle size distribution can be notably decreased by applying closed loop control. Here, the control system manipulated the mill rotation speed. Moreover, it was noticed that significant disturbances, such as drastic changes in the ore type, can require adjustments of the particle size set point to meet the grain size optimality for the mineral indeed.

III) Study of the Control Performance of a Grinding-Flotation Chain

Finally, control of a grinding-flotation process chain was assessed with a simulation model of the Pyhäsalmi grinding – copper flotation circuits. The simulations were based on the dynamic autoregressive models of the grinding section, identified from the process data. The primary mill charge model inputs were: the crushed ore feed rate (t/h) the lumpy ore feed rate (t/h) and the mill power (kW). The grinding circuit outlet particle size model inputs were: the total ore feed rate (t/h), the ratio of the crushed and lumpy ore, the ball mill power (kW) and the pressure of the circuit outlet hydrocyclone (bar). The model set up was accomplished with the primary mill charge – rotation speed – power dependency surface, estimated from the data. In addition, to model the impact of the ground product particle size on the copper flotation performance, a concentrate grade – feed particle size – recovery dependency, shown in Figure 24, was fitted based on the process data.

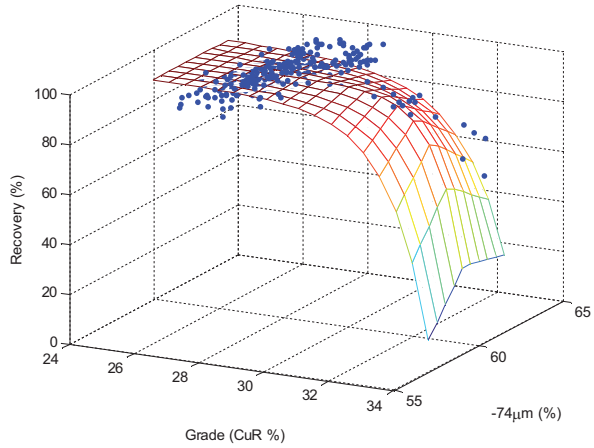

Figure 24. Concentrate recovery (%) vs. grade (%) and the particle size of the feed slurry (under 74 µm fraction, %) at the Pyhäsalmi copper circuit; blue dots are the data (23.-25.10.2008).

The simulation model was operated with a dataset of 4.2.-4.3.2009, consisting of averages on a six-minute basis. As a base case, the *Case A* in Table 6, the simulation was run with the process data only. Instead, in the *Case B* the particle size was controlled and in the *Case C*, in addition to that, also the primary mill charge was controlled in a rule-based manner. The control setup was defined as follows:

- Particle size -74 µm fraction set point: 60%, with target limits: +/- 1%.
- Primary mill charge set point: 42%, with target limits: +/- 1%.
- Particle size is controlled by manipulating the crushed ore with 2.25...0.75 t/h steps.
- Primary mill charge is controlled by manipulating lumpy ore with 0.25 t/h steps.

- Crushed ore is limited between 120...140 t/h.
- Pebble feed is considered to be constant 20 t/h.
- The Cu concentrate grade was set to be 29%.

The process disturbances, representing mainly the ore type variations, were obtained from the original process data. These were: the zero means primary mill charge (%) (summed up with the simulated charge), the ball mill power (kW) and the hydrocyclone feed pressure (bar) (both as an input to the particle size simulation model). The resulting simulated grinding circuit responses as well as the copper flotation responses are summarized in Table 6; the amount of produced copper concentrate increased around 1.7 % from the *Case A* to the *Case C*.

Table 6. Average results of the simulated control cases by using the data based models of the Pyhäsalmi grinding-flotation circuits, the simulations were operated using a process data set 4.2.-4.3.2009.

Simulation Case	Crushed ore (t/h) *MANIPU-LATED VARIABLE*	Lumpy ore (t/h) *MANIPU-LATED VARIABLE*	Total feed rate (t/h)	Primary mill charge (%)	Ground ore particle size fraction <74µm (%)	Cu flotation recovery (%)	Concentrate production (t/h)
A) Simulation run with real process data	130	20	170	41.6	60.0	96.4	5.9
B) Particle size controlled	132	20	172	41.7	59.8	96.5	5.9
C) Particle size and primary mill charge controlled	132	21	173	42.0	59.7	96.5	6.0

Observations Based on the Study

This study briefly demonstrated the impact of the improved grinding circuit control to the subsequent flotation performance. The simulations were carried out by utilizing data-based dynamic and static models. In this case application, stabilization of the primary mill charge closer to the predefined limit increased the mill throughput. In addition, stabilization of the circuit outlet particle size distribution prevented abrupt changes in that, thus reducing occasional recovery losses.

5.4.2 Model-based Control Study for the Siilinjärvi Grinding circuit

At the Siilinjärvi apatite concentrator, changes in the ore type introduce the majority of grinding circuit disturbances. Since the crushed ore is homogenized in heaps, the heap changeovers cause sudden changes in the ore type fed to the grinding circuit. In addition, classification at the ends of the heaps causes often a simultaneous change in the feed size. The subsequent disturbances in the grinding circuit outlet particle size can diminish performance of the following flotation circuit; especially recovery of coarse apatite can be poor. At the studied circuit and control setup (Figure 12), the major constraint was set by the allowed circulating load. At this circuit case, the most powerful variable to control the circulating load is the number of cyclones taken in action.

Requirements for the control system were to be able to manage discrete cyclone pattern control tasks while rejecting the disturbances from the circuit outlet particle size distribution. Therefore, a combination of fuzzy- and model predictive control was set up. The control configuration is shown in Figure 25. Both the ore feed rate (t/h) and the circuit outlet slurry density (kg/dm^3) were the manipulated variables in controlling of the product particle size (%). The disturbance variable was the measured hydrocyclone feed pressure (kPa). Abrupt changes in that were due to changes in the number of operating hydrocyclones. The hydrocyclone valves were manipulated by a fuzzy logic, keeping the circulating load (%) in the predefined limits.

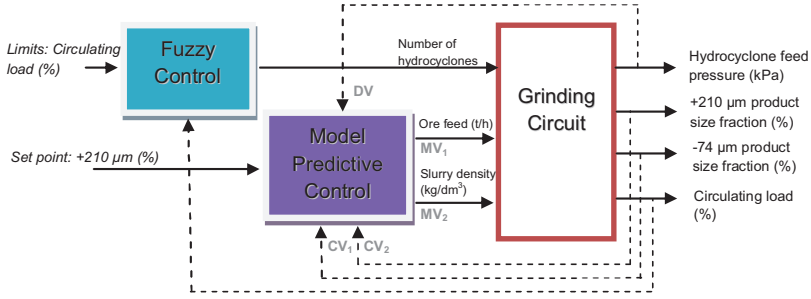

Figure 25. Fuzzy-MPC control scheme to control the circuit product particle size while the circulating load is kept in predefined limits (MPC: DV = disturbance variable, CV = controlled variable, MV = manipulated variable).

The proposed control scheme was set up and tested by simulations; parameterization of the MPC block is presented in [P7]. The MIMO plant model can be presented as follows

$$\begin{bmatrix} y_1(s) \\ y_2(s) \\ y_3(s) \end{bmatrix} = \begin{bmatrix} G_{11}(s) & G_{12}(s) & G_{13}(s) \\ G_{21}(s) & G_{22}(s) & G_{23}(s) \\ G_{31}(s) & G_{32}(s) & G_{33}(s) \end{bmatrix} \begin{bmatrix} u_1(s) \\ u_2(s) \\ u_3(s) \end{bmatrix}, \quad (57)$$

where y_1 and y_2 are the particle size fractions of -74µm (%) and +210µm (%) and y_3 is the circulating load (%); the inputs are: ore feed rate (t/h) u_1, circuit outlet slurry density (kg/dm3) u_2 and hydrocyclone feed pressure (kPa) u_3. The transfer functions $G_{ij}(s)$ were determined based on the experimental data of the Siilinjärvi process. The transfer functions and step responses of them are presented in [P7].

In addition, the reliability of the control system when plant model mismatches were present was verified by set point tracking simulations. Up to 30 % changes both in the model time constants and gain parameters were applied. In addition, up to 1 rel.-% measurement errors were added to the simulated particle size and circulating load values. In all cases the control system was robust; the model errors had notably minor impact on operation in terms of the ISE control index. In practice, the model mismatches occur when the process conditions, especially the feed ore type, change during the daily plant operation.

Finally, the fuzzy – model predictive grinding circuit control scheme was assessed by simulation of around one week period of the plant data. The data (July 21 – 29, 2009) includes five separate ore heaps ran through the mill. In the original data, the ore feed was kept constantly at 480 t/h, slurry density at 1360 kg/dm3, and the number of cyclones at 7 set points. In the control simulation set up, the original measured particle size variation around the mean value was summed with the simulated result, and used further in feedback control. Also, the original measured hydrocyclone pattern feed pressure and circulating load variations were fed to the control system while summed with the simulated results.

Hence, the system was analogous to the scheme shown in Figure 25 where the dotted line feedback signals included also fluctuations obtained from the process data sequence. The set point for the coarse +210 µm fraction was set to 50.6 %, which was the mean value of the process data sequence. The resulting control simulation – in addition of the original process data – for the one week data period is shown in Figure 26.

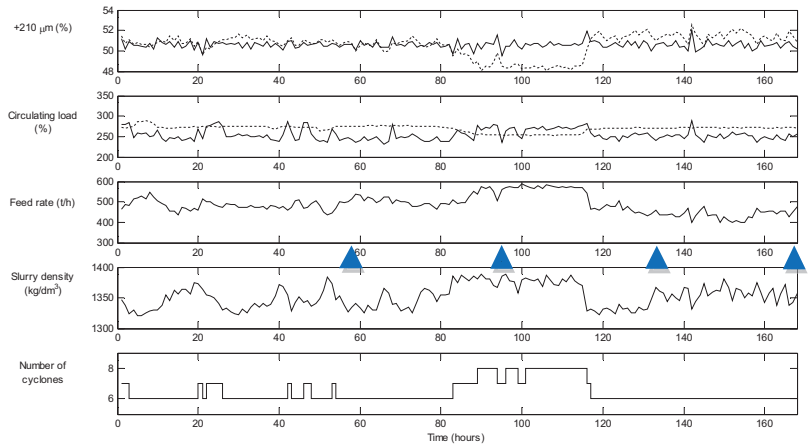

Figure 26. Process data set of the +210 µm (%) particle size fraction and the circulating load (%) (dotted lines), and the simulated results (solid lines) when the feed rate (t/h), the slurry density (kg/dm³) and the number of cyclones - control actions with fuzzy-MPC set up were applied for the same data; changes of the ore heaps are indicated with the triangle symbols.

As a result of the data run, shown in Figure 26, the ore feed rate increased on average 1.8 % within the data period. Meanwhile the variation of the coarse particle size fraction was reduced – for the total dataset 67 % and for processing of one feed ore heap 26 % – apparently still increasing the plant capacity from improved flotation recovery.

Novelty of the Method

A control system for an industrial grinding circuit, incorporating data-based process models and working patterns based on operator knowledge, was formulated. The control assessment pointed out that the model-based control was robust and suitable for drastic ore type changeover management. Moreover, it was discovered that the expected model mismatches did not significantly reduce the control performance. The scheme of fuzzy circulating load control in conjunction with model predictive particle size control has not been presented and verified with an industrially parameterized case elsewhere prior to this.

6 Conclusions

This thesis examines monitoring and control issues of several mineral processing units and process chains. The work covers topics of the state monitoring of a concentrate thickener, the model-based assessment of hindered settling separation and the predictive data based plant-wide monitoring and control studied with grinding and flotation circuits of different setups. In some of the cases the applied methods were tested or implemented in real plant operation and, on the other hand, some of the methods were tested with the aims of the plant data parameterized simulations. Hence, the work included extensively practical plant experiments for gathering the process input - output response data, and the analysis of the data set up the process models. The case plants of this thesis were: the Outokumpu Chrome Oy Kemi Mine, the Yara Suomi Siilinjärvi Mine and the Inmet Mining Co. Pyhäsalmi Mine.

The applied novel model-based techniques provided promising results for all the unit operations and processing circuits focused on in this thesis. The obtained results can be directly used in plant practices by adopting the model-based information as a part of the process operation, using the process models for equipment design, scale-up and troubleshooting, and also, by utilizing the proposed new control setups. The common factor in all the studied cases is that the operation of the processes depends strongly on the particle size distribution of the processed material. This addresses the importance of stable and optimized operation of the grinding circuit of a concentrator. This has been the key theme in the studies of the grinding-concentration chains of all of the cases.

In this thesis, the most extensive grinding circuit control study focused on the Siilinjärvi apatite ore concentrator. The proposed model predictive particle size control with fuzzy circulating load control gave good results when simulating several ore heap changeovers with the plant data. The control system managed to reduce the long term fluctuation of the coarse particle size fraction significantly when running the process from one feed type to another. Even during the processing of one ore type (one separate heap) the simulated reduction in the slurry particle size variation was well over 20 %. The economic impact of that in the minerals processing recovery is obvious. Based on the observations of the clustered long term plant data, for a certain ore type, even 2 %-unit increment in the coarse slurry size fraction can lead to nearly 1 % losses in recovery. On a yearly basis, this is a

significant loss due to high throughput volumes of ore processing plants, even if the number itself seems to be small.

When comparing different types of process model based control methods, the data based methods offers an attractive way to construct the plant model with standard mathematical forms. In large systems the fuzzy controls can be time consuming to tune up. Therefore, among the applied methods here, the model predictive control is considered to be preferable. However, the most reliable model based controls for minerals processing applications are achieved with predictive models, which are based on mineralogical setup of the feed composition and include unit process models treading the material based on their physical and chemical characteristics. Such a control system can be preferably accomplished with soft-sensors based on similar models with mineralogical properties. Parameter estimation techniques, such as Kalman filtering, can offer proven methods for reliable model adaptation for the model on-line usage.

In general, this thesis suggests a more extensive use of unit models and plant-wide process models in the plant design and control. Around a decade ago Lynch and Morrison (1999) predicted that dynamic mineral process simulators will be utilized more and more commonly in automatic control and for operator training purposes. This work showed that the model-based approaches can indeed provide highly useful estimates of the unmeasured states. Also the predictive use of models can bring the concentrator control closer to the optimum. Especially they provide valuable support for operators in the making of correct control decisions.

References

Aaltonen, J. (2010), communication in MinMo project final meeting 9.2.2010, Outotec Espoo.

Alexander, D.J., Franzidis, J.P. and Manlapig, E.V. (2003). Froth recovery measurement in plant scale flotation cells, *Miner. Eng.,* **16**, pp. 1197-1203.

Allenius, H., Oravainen, H. and Virtanen, M. (2008). How much can we afford to invest?, *Proceedings of the XXIV International Mineral Processing Congress*, Beijing, China, 24.-28. Sep., pp. 4191-4198.

Apelt, T.A. and Thornhill, N.F. (2009). Inferential measurement of SAG mill parameters V: MPS simulation*, Miner. Eng.*, **22**, pp. 1045-1052.

Atasoy, Y. and Spottiswood, D.J. (1995). A study of particle separation in a spiral concentrator, *Miner. Eng.*, **8**, pp. 1197-1208.

Bequette, B.W. (2003). *Process Control Modeling, Design, and Simulation*, Prentice Hall, New Jersey, 769 p.

Bequette, B.W. (2007). Non-linear model predictive control: a personal retrospective, *Can. J. Chem. Eng.*, **85**, pp. 408-414.

Bergh, L.G., Yianatos, J.B. and Leiva, C.A. (1998). Fuzzy supervisory control of flotation columns, *Miner. Eng.*, **11**, pp. 739-748.

Bergh, L.G., Yianatos, J.B., Acuña, C.A., Pérez, H. and López, F. (1999). Supervisory control at Salvador flotation columns, *Miner. Eng.*, **12**, pp. 733-744.

Brochot, S., Wiegel, R.L., Ersayin, S. and Touze S. (2006). Modeling and simulation of comminution circuits with USIM PAC, In: *Advances in comminution* (Edit. Kawatra S.K.), Society for Mining, Metallurgy and Exploration, Inc. (SME), Littleton, pp. 495-511.

Burt, R.O. (1984). *Developments in Mineral Processing 5, Gravity Concentration Technology*, Elsevier, Amsterdam, 605 p.

Carvalho, M.T., and Durão, F. (2002). Control of a flotation column using fuzzy logic inference, *Fuzzy Set. Syst.*, **125**, pp. 121-133.

Chhabra, R.P., Agarwal, L. and Sinha N.K. (1999). Drag on non-spherical particles: an evaluation of available methods*, Powder Technol.,* **101**, pp. 288-295.

Cipriano, A. (2010). Industrial products for advanced control of mineral processing plants, In: *Advances in Industrial Control, Advanced Control and Supervision of Mineral Processing Plants* (Edit. Sbárbaro, D. and Villar, R.), Springer, London, pp. 287-308.

Coetzee, L.C., Craig, I.K. and Kerrigan, E.C. (2010). Robust Nonlinear Model Predictive Control of a Run-of-Mine Ore Milling Circuit, *IEEE Transactions on Control Systems Technology*, **18**, pp. 222-229.

Concha, F., Bürger, R. (2003). Thickening in the 20th century: a historical perspective, *Miner. & Metall. Process.*, 20, pp. 57-67.

Dahlke, R., Gomez, C. and Finch, J.A. (2005). Operating range of a flotation cell determined from gas holdup vs. gas rate, *Miner. Eng.,* **18**, pp. 977-980.

Das A., Sarkar B. and Mehrotra S.P. (2009). Prediction of separation performance of Floatex Density Separator for processing of fine coal particles, *Int. J. Miner. Process.*, **91**, pp. 41-49.

Datta, A. and Rajamani, R.K. (2002). A direct approach of modeling batch grinding inball mills using population balance principles and impact energy distribution, *Int. J. Miner. Process.*, **64**, pp. 181-200.

Dayal, B.S. and MacGregor, J.F. (1997a). Improved PLS algorithms, *J. Chemom.*, **11**, pp. 73-85.

Dayal, B.S. and MacGregor, J.F. (1997b). Recursive exponentially weighted PLS and its applications to adaptive control and prediction*, J. Process Control*, **7**, pp. 169-179.

de V. Groenewald, J.W., Coetzer, L.P. and Aldrich, C. (2006). Statistical monitoring of a grinding circuit: an industrial case study, *Miner. Eng.,* **19**, pp. 1138-1148.

Duarte, M., Sepúlveda, F., Redard, J.P., Espinoza, P., Lazcano, V., Castillo A., Zorbas, A., Giménez, P. and Castelli, L. (1998). Grinding operation optimization of the Codelco-Andina concentrator plant, *Miner. Eng.,* **11**, pp. 1119-1142.

Duarte, M., Suárez, A. and Bassi, D. (2001). Control of grinding plants using predictive multivariable neural control, *Powder Technol.*, **115**, pp. 193-206.

Duchesne, C. (2010). Multivariate image analysis in mineral processing, In: *Advanced Control and Supervision of Mineral Processing Plants (Ed. Sbarbaro, D. and del Villar, R.)*, Springer, London, pp 85-142.

Estrada-Ruiz, R.H. and Pérez-Garibay, R. (2009). Evaluation of models for air recovery in a laboratory flotation column, *Miner. Eng.,* **22**, pp. 1193-1199.

Farrow, J.B., Jonston, R.R.M., Simic, K. and Swift, J.D. (2000). Consolidation and aggregate densification during gravity thickening, *Chem. Eng. J.*, **80**, pp. 141-148.

Felice, R.D. (1995). Hydrodynamics of liquid fluidization. Review article number 47, *Chem. Eng. Sci.*, **50**, pp. 1213-1245.

Findeisen, R. and Allgöwer, F. (2002). An introduction to nonlinear model predictive control, *Book of Abstract of the 21st Benelux Meeting on Systems and Control,* 19.-21. March, Veldhoven, Netherlands, pp. 119-141.

Fortescue, T.R., Kershenbaum, L.S. and Ydstie, B.E. (1981). Implementation of self-tuning regulators with variable forgetting factors, *Automatica*, **17**, pp. 831-835.

Galvin, K.P., Pratten, S. and Nquyen Tran Lam, G. (1999a). A generalized empirical description for particle slip velocities in liquid fluidized beds, *Chem. Eng. Sci.*, **54**, pp. 1045-1052.

Galvin, K.P., Pratten, S.J. and Nicol, S.K. (1999b). Dense medium separation using a teetered bed separator, *Miner. Eng.,* **12**, pp. 1059-1081.

Garrido, C.Q. and Sbarbaro, D. (2009). Multivariable Model Predictive Control of a Simulated SAG plant, *Proceedings of IFAC MMM workshop*, 14.-16.th Oct. 2009, Viña del Mar, Chile, 6 p.

Garrido, C.Q. and Sbarbaro, D.H. (2009). Multivariable Model Predictive Control of a Simulated SAG plant, *Proceedings of IFAC MMM workshop*, 14.-16.th Oct. 2009, Viña del Mar, Chile, 6 p.

Gatica, J.H., Ramos, B.G., Villalobos, J.E. and Olivares, J.F. (2009). Robust Multivariable Predictive Control Strategy on SAG Mills; Codelco Chile – Division El Teniente, *Proceedings of IFAC MMM workshop*, 14.-16.th Oct. 2009, Viña del Mar, Chile, 6 p.

Geological Survey of Finland (2010a), *Industrial minerals and rocks*, http://en.gtk.fi/ExplorationFinland/Commodities/IndustrialMinerals.html.

Geological Survey of Finland (2010b), *Kemi mine*, http://en.gtk.fi/ExplorationFinland/Moreinfo/kemi.html.

Gonzalez, G.D., Miranda, D., Casali, A. and Vallebuona, G. (2008). Detection and identification of ore grindability in a semiautogenous

grinding circuit model using wavelet transform variances of measured variables, *Int. J. Miner. Process.*, **89**, pp. 53–59.

Gorain, B.K., Franzidis, J.-P. and Manlapig, E.V. (1995a). Studies on impeller type, impeller speed and air flow rate in an industrial scale flotation cell – part 1: effect on bubble size distribution, *Miner. Eng.,* **8**, pp. 615-635.

Gorain, B.K., Franzidis, J.-P. and Manlapig, E.V. (1995b). Studies on impeller type, impeller speed and air flow rate in an industrial scale flotation cell – part 2: effect on gas holdup, *Miner. Eng.,* **8**, pp. 1557-1570.

Gorain, B.K., Franzidis, J.-P. and Manlapig, E.V. (1996). Studies on impeller type, impeller speed and air flow rate in an industrial scale flotation cell – part 3: effect on superficial gas velocity, *Miner. Eng.,* **9**, pp. 639-654.

Gorain, B.K., Franzidis, J.-P. and Manlapig, E.V. (1998). Studies on impeller type, impeller speed and air flow rate in an industrial scale flotation cell – part 5: validation of k-S_b relationship and effect of froth depth, *Miner. Eng.,* **11**, pp. 615-626.

Gorain, B.K., Franzidis, J.-P. and Manlapig, E.V. (1999). The empirical prediction of bubble surface area flux in mechanical flotation cells from cell design and operating data, *Miner. Eng.,* **12**, pp. 309-322.

Grau, R.A., Laskowski, J.S. and Heiskanen, K. (2005). Effect of frothers on bubble size, *Int. J. Miner. Process.,* **76**, pp. 225–233.

Grewal, M.S. and Andrews, A.P. (2008). *Kalman filtering: theory and practice using MATLAB, 3rd edition*, Wiley, New York, 676 p.

Hartman, M., Havlin, V., Trnka, O. and Carsky, M. (1989). Predicting the free fall velocities of spheres, *Chem. Eng. Sci.*, **44**, pp. 1743–1745.

Hartman, M., Trnka, O. and Svoboda, K. (1994), Free settling of nonspherical particles, *Ind. Eng. Chem. Res.*, **33**, pp. 1979-1983.

Heiskanen, K. (1993). *Particle Classification*, Chapman & Hall, London, 350 p.

Hodouin, D. (2010). Methods for automatic control, observation, and optimization in mineral processing plants, *J. Process Contr.*, 21, pp. 211-225.

Hodouin, D., Bazin, C., Gagnon, E. and Flament, F. (2000). Feedforward-feedback predictive control of a simulated flotation bank, *Powder Technol.*, **108**, pp. 173-179.

Holland-Batt, A.B. (1989). Spiral separation: theory and simulation. *Trans. Instn. Min. Metall. Sect. C: Mineral Process. Extr. Metall.,* **98**, C46–C60.

Holland-Batt, A.B. (2009). A method for the prediction of the primary flow on large diameter spiral troughs, *Miner. Eng.*, **22**, pp. 352-356.

Huhtelin, T. (2007). *Day 6: The Kemi layered intrusion and the Kemi chrome mine, In: Metallogeny and tectonic evolution of the northern Fennoscandian Shield: field trip guidebook*, Geologian tutkimuskeskus, Opas 54, Espoo, pp. 85-90.

Hyötyniemi, H. (2001). Multivariate regression – techniques and tools. Technical Report 125, Helsinki University of Technology, Control Engineering Laboratory, 207 p.

Inmet Mining Co. (2010). *Annual report 2009*, http://www.inmetmining.com/Theme/Inmet/files/pdf/2009%20Annual%20Report_Pyhasalmi.pdf.

Johnston, R.R.M., Simic, K. (1991). Improving thickener operation and control by means of a validated model, *Miner. Eng.*, **4**, pp. 695-705.

Jones, R.M. (2003). Particle Size Analysis By Laser Diffraction: ISO 13320, Standard Operating Procedures, and Mie Theory, *American Laboratory*, January 2003, pp. 44-47.

Kalman, R.E. (1960). A New Approach to Linear Filtring and Prediction Problems, *Journal of Basic Engineering*, March 1960, pp. 35-45.

Kemira (2005), *Kemira Grow-How Suomessa* (brochure, available in: http://www.kemira-growhow.com/NR/rdonlyres/C13494BA-69C9-4C60-858F-DF8B774C42F9/0/KGHesiteSUOMI.pdf), 14 p.

King, R.P. (2001). *Modeling and Simulation of Mineral Processing Systems*, Butterworth-Heinemann, Oxford, 403 p.

Lamberg, P. (2010). Structure of a Property Based Simulator for Minerals and Metallurgical Industry, *Proceedings of SIMS 2010*, 13-14 Oct. 2010, Oulu, Finland, 5 p.

Lamberg, P., Paloranta, S., Aaltonen, A. and Myllykangas, H. (2009). A property based model of flotation and application in a dynamic simulator for training purposes, *Proceedings of the 48th annual conference of metallurgists of CIM*, 23.-26.th Aug., Sudbury, Ontario, Canada, pp. 229-240.

Lestage, R., Pomerleau, A. and Hodouin, D. (2002). Constrained real-time optimization of grinding circuit using steady-state linear programming supervisory control, *Powder Technol.*, **124**, pp. 254-263.

Lin, C-T. and Lee, G. (1996). *Neural fuzzy systems: a neuro-fuzzy synergism to intelligent systems*, Prentice Hall,Upper Saddle River, 797 p.

Love, J. (2007). *Process Automation Handbook – A Guide to Theory and Practice*, Springer, London, 1093 p.

Loveday, G.K. and Cilliers, J.J. (1994). Fluid flow modeling on spiral concentrators, *Miner. Eng.*, **7**, pp. 223-237.

Lynch, A.J. (1977), *Developments in Mineral Processing 1, Mineral crushing and grinding circuits*, Elsevier, Amsterdam, 342 p.

Lynch, A.J. and Morrison, R.D. (1999). Simulation in mineral processing history, present status and possibilities, *J. S. Afr. I. Min. Metall.*, **99**, pp. 283-288.

MacGregor, J.F. and Kourti, T. (1995). Statistical process control of multivariate processes, *Control Eng. Pract.*, **3**, pp. 403-414.

Mäki, T. (2008). Pyhäsalmen kaivos – kaivosgeologiaa 50 vuotta, *Geologi*, 60, pp. 132-133. (in Finnish)

McCabe, W., Smith, J. and Harriot, P. (1993). *Unit Operations of Chemical Engineering*, 5th ed., McGraw-Hill, New York, 1130 p.

McCaffery, KM, Katom, M and Craven, JW, (2002). Ongoing evolution of advanced SAG mill control at Ok Tedi, *Minerals & Metallurgical Processing*, **19**, pp. 72-80.

Mitra, K. (2009). Multiobjective optimization of an industrial grinding operation under uncertainty, *Chem. Eng. Sci.*, **64**, pp. 5043-5056.

Moritz, D., Ferreau, H.J. and Haverbeke, N. (2008). Efficient Numerical Methods for Nonlinear MPC and Moving Horizon Estimation, *Int. Workshop on Assessment and Future Directions of NMPC*, 5.-9. Sep., Pavia, Italy.

Morrison, R., Loveday, B., Djordjevic, N., Cleary, P. and Owen, P. (2006). Linking discrete element modeling to breakage in a pilot-scale AG/SAG mill, In: *Advances in comminution* (Edit. Kawatra S.K.), Society for Mining, Metallurgy and Exploration, Inc. (SME), Littleton, pp. 269-283.

Muller, B. and de Vaal, P.L. (2000). Development of model predictive controller for a milling circuit, *Journal of the South African Institute of Mining and Metallurgy*, **100**, pp. 449-453.

Napier-Munn, T.J., Morrel, S., Morrison, R.D. and Kojovic, T. (2005). *Mineral comminution circuits – their operation and optimization*, JKMRC, 2005, 413 p.

Neethling, S.J. and Cilliers, J.J. (2008). Predicting air recovery in flotation cells, *Miner. Eng.,* **21**, pp. 937-943.

Neethling, S.J. and Cilliers, J.J. (2009). The entrainment factor in froth flotation: Model for particle size and other operating parameter effects, *Int. J. Miner. Process.*, **93**, pp. 141-148.

Neethling, S.J., Lee, H.T. and Chilliers J.J. (2003). Simple relationships for predicting the recovery of liquid from flowing foams and froths, *Miner. Eng.,* **16**, pp. 1123-1130.

Nesset, J.E., Hernandez-Aguilar, J.R., Acuna, C., Gomez, C.O. and Finch J.A. (2006). Some gas dispersion characteristics of mechanical flotation machines, *Miner. Eng.,* **19**, pp. 807-815.

Nieto, L., Olivares, J., Gatica, J., Ramos, B. and Olmos, H. (2009). Implementation of a Multivariable Controllers for Grinding-Classification Process, *Proceedings of IFAC MMM workshop*, 14.-16.th Oct. 2009, Viña del Mar, Chile, 6 p.

Núñez, F., Tapia, L. and Cipriano, A. (2010). Hierarchical hybrid fuzzy strategy for column flotation control, *Miner. Eng.*, **23**, pp. 117-124.

Perry, R.H. and Green, D.W. (2008). *Perry's chemical engineers' handbook*, 8th ed., McGraw-Hill, New York, 2703 p.

Pokrajcic, Z. and Morrison, R. (2008). A Simulation Merhodology for the Design of Eco-efficient Comminution Circuits, *Proceedings of the XXIV International Mineral Processing Congress*, Beijing, China, 24.-28.th Sep., pp. 481-495.

Pomerleau, A., Hodouin, D., Despiens, A. and Gagnon, E. (2000). A survey of grinding circuit control methods: from decentralized PID controllers to multivariable predictive controllers, *Powder Technol.*, **108**, pp. 103-115.

Powell, M.S. and McBride (2006). What is required from DEM simulations to model breakage in mills?, *Miner. Eng.,* **19**, pp. 1013-1021.

Powell, M.S., Govender, I. and McBride, A.T. (2008). Applying DEM outputs to the unified comminution model, *Miner. Eng.,* **21**, pp. 744-750.

Prasher, C.L. (1987). *Crushing and Grinding Process Handbook*, Wiley, New York, 474 p.

Qin, S.J. and Badgwell, T.A. (2003). A survey of industrial model predictive control technology, *Control Eng. Pract.*, **11**, pp. 733-764.

Ramasamy, M., Narayanan, S.S. and Rao, Ch.D.P. (2005), Control of ball mill grinding circuit using model predictive control scheme, *J. Process. Contr.*, **15**, pp. 273-283.

Rawlings, J.B. (2000). Tutorial Overview of Model Predictive Control, IEEE Control Systems Magazine, June 2000, pp. 38-52.

Reuter, M.A., Heiskanen, K., Boin, U., van Schaik, A., Verhoef, E., Yang, Y. and Georgalli, G. (2005). *Developments in Mineral Processing 16, The metrics of material and metal ecology: Harmonizing the Resource, Technology and Environmental Cycles*, Edit. Wills, B.A., Elsevier, Amsterdam, 706 p.

Rhodes, M. (1998). *Introduction to Particle Technology*, Wiley, Chichester, 320 p.

Rowe, P.N. (1987). A convenient empirical equation for estimation of the Richardson-Zaki exponent, *Chem. Eng. Sci.*, **42**, pp. 2795-2796.

Rudman, M., Paterson, D.A. and Simic, K. (2010). Efficiency of raking in gravity thickeners, *Int. J. Miner. Process.*, **95**, pp. 30-39.

Rudman, M., Simic, K., Paterson D.A., Strode, P., Brent A. and Sutalo, I.D. (2008). Raking in gravity thickeners, *Int. J. Miner. Process.*, **86**, pp.114-130.

Saltikoff, B., Puustinen, K. and Tontti, M. (2006). *Metallogenic zones and metallic mineral deposits in Finland : explanation to the Metallogenic map of Finland*, Geological Survey of Finland, Special Paper 35, Espoo, ISBN 951-690-852-7, 66 p.

Sarkar, B. and Das, A. (2010). A comparative study of slip velocity models for the prediction of performance of floatex density separator, *Int. J. Miner. Process.*, **94**, pp. 20-27.

Sarkar, B., Das A. and Mehrotra S.P. (2008), Study of separation features in floatex density separator for cleaning fine coal, *Int. J. Miner. Process.*, **86**, pp. 40-49.

Savassi, O.N. (2005). A compartment model for the mass transfer inside a conventional flotation cell, *Int. J. Miner. Process.*, **77**, pp. 65-79.

Savassi, O.N., Alexander, D.J., Franzidis, J.P. and Manlapig, E.V. (1998). An empirical model for entrainment in industrial flotation plants, *Miner. Eng.*, **11**, pp. 243-256.

Sbárbaro, D. and Villar, R. (editors) (2010). *Advances in Industrial Control, Advanced Control and Supervision of Mineral Processing Plants*, Springer, London, 310 p.

Smith, C. and Clilliers, J. (2010). Predicting water recovery from flotation cells, *Proceedings of XXV IMPC*, Brisbane, Australia, pp. 2367-2373.

Smith, C., Neethling, S. and Cilliers, J.J. (2008). Air-rate profile optimization: From simulation to bank improvement, *Miner. Eng.,* **21**, pp. 973-981.

Smith, C.D., Hadler, K., and Cilliers, J.J. (2010). Flotation bank air addition and distribution for optimal performance, *Miner. Eng.,* **23**, pp. 1023-1029.

Sorenson, H.W. (1985). Least-squares estimation: from Gauss to Kalman, *Kalman Filtering: Theory and Application* (ed. Sorenson, H.W.), IEEE Press, New York, pp. 7-12.

Tuzcu, E.T. and Rajamani, R.K. (2011). Modeling breakage rates in mills with impact energy spectra and ultra fast load cell data, *Miner. Eng.,* **24**, pp. 252-260.

Venkoba Rao, B. (2007). Extension of particle size stratification model to incorporate particle size effects, *Int. J. Miner Process*, **85**, pp. 50-58.

Venkoba Rao, B. and Kapur, P.C. (2008). Simulation of multi-stage gravity separation circuits by size-density bivariate partition function, *Int. J. Miner. Process.*, **89**, 2008, pp. 23-29.

Venkoba Rao, B., Kapur, P.C. and Konnur R. (2003). Modeling the size-density partition surface of dense-medium separators, *Int. J. Miner. Process.*, **72**, pp. 443-453.

Webmineral (2010). *Mineralogy Database*, http://www.webmineral.com.

Wei, D. and Craig, I.K. (2009a). Economic performance assessment of two ROM ore milling circuit controllers, *Miner. Eng.*, **22**, pp. 826-839.

Wei, D. and Craig, I.K. (2009b). Grinding mill circuits – a survey of control and economic concerns, *Int. J. Miner. Process.,* **90**, pp. 56–66.

Welch, G. and Bishop, G. (2006). An Introduction to the Kalman Filter, TR 95-041 Univ. of North Carolina at Chapel Hill, 16 p.

Welsby, S.D.D., Vianna, S.M.S.M. and Franzidis, J.-P. (2010). Assigning physical significance to floatability components, *Int. J. Miner. Process.,* **97**, pp. 59–67.

Wills, B.A. and Napier-Munn, T. (2006). *Will's Mineral Processing Technology*, 7th ed., Butterworth-Heinemann, Amsterdam, 444 p.

Wold, S., Sjöström, M. and Eriksson, L. (2001). PLS-regression: a basic tool of chemometrics, *Chemometr. Intell. Lab.*, **58**, pp. 109-130.

Yara (2010). *Production – Siilinjärvi, Finland*, http://www.yara.com/about/where_we_operate/finland_production_siilinjarvi.aspx.

Yianatos, J. and Contreras, F. (2010). Particle entrainment model for industrial flotation cells, *Powder Technol*., **197**, pp. 260-267.

Yianatos, J.B., Bergh, L.G. and Aguilera, J. (2000). The effect of grinding on mill performance at division Salvador, Codelco-Chile, *Miner. Eng*., **13**, pp. 485-495.

Yianatos, JB, lisboa, MA and Baeza, DR (2002). Grinding capacity enhancement by solid concentration control of hydrocyclone underflow, *Miner. Eng*., **15**, pp. 317-323.

Zheng, X., Franzidis, J.P. and Johnson, N.W. (2006a). An evaluation of different models of water recovery in flotation, *Miner. Eng.,* **19**, pp. 871-882.

Zheng, X., Johnson, N.W. and Franzidis J.-P. (2006). Modeling of entrainment in industrial flotation cells: Water recovery and degree of entrainment, *Miner. Eng.,* **19**, pp. 1191-1203.

Zigrang, D.J. and Sylvester, N.D. (1981). An explicit equation for particle settling velocities in solid liquid systems, *AIChE J*., **27**, pp. 1043–1044.

Appendix - Publications

Aalto-DD 17/2012

ISBN 978-952-60-4511-5
ISBN 978-952-60-4512-2 (pdf)
ISSN-L 1799-4934
ISSN 1799-4934
ISSN 1799-4942 (pdf)

Aalto University
School of Electrical Engineering
Department of Automation and Systems Technology
www.aalto.fi

BUSINESS +
ECONOMY

ART +
DESIGN +
ARCHITECTURE

SCIENCE +
TECHNOLOGY

CROSSOVER

DOCTORAL
DISSERTATIONS